Atmospheric
Chemistry
and Physics

Research article

Temperature-dependent aqueous OH kinetics of C_2–C_{10} linear and terpenoid alcohols and diols: new rate coefficients, structure–activity relationship, and atmospheric lifetimes

Bartłomiej Witkowski, Priyanka Jain, Beata Wileńska, and Tomasz Gierczak

University of Warsaw, Faculty of Chemistry, al. Żwirki i Wigury 101, 02-089 Warsaw, Poland

Correspondence: Bartłomiej Witkowski (bwitk@chem.uw.edu.pl)

Abstract. Aliphatic alcohols (AAs), including terpenoic alcohols (TAs), are ubiquitous in the atmosphere due to their widespread emissions from natural and anthropogenic sources. Hydroxyl radical (OH) is the most important atmospheric oxidant in both aqueous and gas phases. Consequently, the aqueous oxidation of the TAs by the OH inside clouds and fogs is a potential source of aqueous secondary organic aerosols ($_{aq}$SOAs). However, the kinetic data, necessary for estimating the timescales of such reactions, remain limited. Here, bimolecular rate coefficients ($k_{OH_{aq}}$) for the aqueous oxidation of 29 C_2–C_{10} AAs by hydroxyl radicals (OH) were measured with the relative rate technique in the temperature range 278–328 K. The values of $k_{OH_{aq}}$ for the 15 AAs studied in this work were measured for the first time after validating the experimental approach. The $k_{OH_{aq}}$ values measured for the C_2–C_{10} AAs at 298 K ranged from 1.80×10^9 to 6.5×10^9 $M^{-1} s^{-1}$. The values of activation parameters, activation energy (7–17 $kJ\,mol^{-1}$), and average Gibbs free energy of activation ($18 \pm 2\,kJ\,mol^{-1}$) strongly indicated the predominance of the H-atom abstraction mechanism. The estimated rates of the complete diffusion-limited reactions revealed up to 44 % diffusion contribution for the C_8–C_{10} AAs.

The data acquired in this work and the values of $k_{OH_{aq}}$ for AAs, carboxylic acids, and carboxylate ions available in the literature were used to develop a modified structure–activity relationship (SAR). The SAR optimized in this work estimated the temperature-dependent $k_{OH_{aq}}$ for all compounds under investigation with much higher accuracy compared to the previous models. In the new model, an additional neighboring parameter was introduced ($F \geq (CH_2)_6$), using the $k_{OH_{aq}}$ values for the homolog (C_2–C_{10}) linear alcohols and diols. A good overall accuracy of the new SAR at 298 K (slope $= 1.022$, $R^2 = 0.855$) was obtained for the AAs and carboxylic acids under investigation. The kinetic database ($k_{OH_{aq}}$ values in this work and compiled literature data) was also used to further enhance the ability of SAR to predict temperature-dependent values of $k_{OH_{aq}}$ in the temperature range 278–328 K.

The calculated atmospheric lifetimes indicate that terpenoic alcohols and diols can react with the OH in aerosol, cloud, and fog water with liquid water content (LWC) $\geq 0.1\,g\,m^{-3}$ and LWC $\geq 10^{-4}\,g\,m^{-3}$, respectively. The preference of terpenoic diols to undergo aqueous oxidation by the OH under realistic atmospheric conditions is comparable with terpenoic acids, making them potentially effective precursors of $_{aq}$SOAs. In clouds, a decrease in the temperature will strongly promote the aqueous reaction with the OH, primarily due to the increased partitioning of WSOCs into the aqueous phase.

1 Introduction

Biogenic volatile organic compounds (BVOCs) account for 20 %–90 % of the global emissions of non-methane organics into the atmosphere, consisting primarily of isoprene and terpenes, which are emitted by vegetation (Sindelarova et al., 2022). The oxidation of these atmospherically abundant BVOCs in the gas phase is one of the major sources of secondary organic aerosols (SOAs), which are formed by the nucleation of the low-volatility, oxygenated products and their condensation onto the existing particles (Hallquist et al., 2009).

SOAs account for a large fraction of organic aerosol (OA) mass, which contributes up to 90 % of fine (submicron) particulate matter (PM) (Jimenez et al., 2009; Xu et al., 2021). SOAs are important climate-forcing agents; they alter the properties of clouds, which in turn affects the Earth's hydrological cycle (Mahilang et al., 2021; Shrivastava et al., 2017). Furthermore, SOAs absorb and scatter solar radiation, thereby affecting the Earth's radiation balance and visibility (Tsigaridis and Kanakidou, 2018). Additionally, inhalation of fine PM has been associated with cardiovascular and respiratory conditions, resulting in increased mortality (Pye et al., 2021).

There are still many uncertainties regarding the formation, evolution, and climate forcing of SOAs, which greatly limits the current understanding of the present and future environmental impacts of aerosols (Shrivastava et al., 2017; Fuzzi et al., 2015; Mahilang et al., 2021). Historically, gas-phase oxidation of BVOCs was considered the major source of SOA in the atmosphere (Hallquist et al., 2009). More recently, the aqueous and multiphase reactions of atmospherically abundant water-soluble organic compounds (WSOCs) have been recognized as atmospherically relevant processes (Su et al., 2020; Carlton et al., 2020). These aqueous and multiphase reactions, although still not well characterized, are expected to significantly contribute to the formation of atmospheric SOAs (Ervens et al., 2018; McVay and Ervens, 2017; McNeill, 2015). For instance, the formation of SOAs in the aqueous phase (referred to as $_{aq}$SOAs) can, in part, explain the discrepancies between observed and modeled budgets of OAs (Su et al., 2020; Pai et al., 2020; Lin et al., 2014; Tsui et al., 2019).

Alcohols are one of the major classes of WSOCs in the atmosphere; they are emitted from both natural and anthropogenic sources (Mellouki et al., 2015) and include short- and longer-chain (fatty) linear alcohols and diols, as well as cyclic and terpenoic alcohols (TAs) (Guenther et al., 2012; Chen et al., 2021; Konjeviæ et al., 2023). In the atmosphere, hydroxyl radical (OH) is the most important daytime oxidant (Herrmann et al., 2015; Mahilang et al., 2021). Consequently, the aliphatic WSOCs, including AAs, are expected to react primarily with OH and nitrate radicals (NO_3) (Mellouki et al., 2015). In addition to reaction in the gas phase (Ceacero-Vega et al., 2012), AAs can also undergo aqueous oxidation

by the OH – $R(I)$ – inside the aqueous particles, depending on their Henry's law constants (H) and liquid water content (LWC, $g\,m^{-3}$) of clouds, fogs, and aerosols (Sander, 2015; Herrmann et al., 2015).

$$AA + OH_{aq} \rightarrow products\ R(I).$$
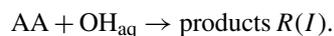
Consequently, in the atmospheric aqueous droplets, $R(I)$ can yield low-volatility products, including carboxylic (terpenoic) acids (Witkowski et al., 2023; Yasmeen et al., 2011). Therefore, TAs (and diols) may be efficient precursors of $_{aq}$SOAs. Due to their larger carbon backbones (C_7–C_{10}) and cyclic structures, TAs have the potential to undergo $R(I)$ without extensive fragmentation (Ceacero-Vega et al., 2012). However, to date, there have not been many studies that investigated the aqueous OH kinetics of TAs (Herrmann et al., 2009, 2015; Gligorovski et al., 2009; Leviss et al., 2016).

To evaluate whether or not a reaction with the OH is a relevant removal pathway for a given molecule under realistic atmospheric conditions, chemical models are utilized (Zhu et al., 2020; Bräuer et al., 2019). Bimolecular reaction rate coefficients for the reaction of organic compounds with the OH in the gas ($k_{OH_{gas}}$) and in the aqueous ($k_{OH_{aq}}$) phases are the foundation of both simple and complex chemical models (Herrmann et al., 2015) used in the field of atmospheric chemistry to investigate the reaction pathways for various WSOCs (Zhu et al., 2020).

Following decades of extensive research, gas-kinetic databases are available for the reactions of various VOCs with atmospherically abundant oxidants (McGillen et al., 2020, 2021). On the other hand, the currently available aqueous kinetic datasets are still limited and contain primarily room-temperature data (Buxton et al., 1988; Herrmann et al., 2015). Reliable kinetic datasets are crucial for an accurate parametrization of the complex aqueous and multiphase reactions, which are directly connected with the formation and processing of $_{aq}$SOAs in the atmosphere (Bräuer et al., 2019; Ervens, 2015).

In this work, after validating the experimental approach, the values of $k_{OH_{aq}}$ for linear and terpenoic AAs and diols were measured with the relative rate technique. Here, $k_{OH_{aq}}$ for multiple AAs were measured in a single experiment; $R(I)$ was carried out in a bulk reactor and the concentrations of individual AAs in the reaction solution were measured with gas chromatography (Herrmann et al., 2005). Because the temperature range in the atmosphere extends above and below room temperature, the kinetic measurements were carried out in the temperature range between 278 and 323 K.

However, measuring the k_{OH} values for the numerous WSOCs present in the environment is unfeasible (Goldstein and Galbally, 2007). Consequently, structure–activity relationships (SARs) are widely utilized in the field of atmospheric chemistry for estimating the k_{OH} values of various organic molecules based on their molecular structures (Monod and Doussin, 2008; Kwok and Atkinson, 1995). At

the same time, the ability of current aqueous SARs to predict the temperature-dependent $k_{OH_{aq}}$ values for the WSOCs with larger carbon backbones remain limited (Herrmann et al., 2005; Bräuer et al., 2019). Moreover, the methodology used in the current aqueous SARs was developed for predicting the values of $k_{OH_{gas}}$. Therefore, it is still unclear whether or not this approach is entirely adequate for estimating the rates of aqueous reactions (Monod and Doussin, 2008; Kwok and Atkinson, 1995).

The kinetic data acquired in this work and the compiled literature data were used to develop a modified kinetic SAR for predicting the values of $k_{OH_{aq}}$ for AAs, carboxylic acids, and carboxylate ions at different temperatures. Subsequently, the atmospheric lifetimes for the five TAs under investigation due to $R(I)$ were estimated to evaluate their potential to yield $_{aq}$SOAs under realistic atmospheric conditions.

2 Materials and methods

Materials and reagents are listed in Sect. S1 in the Supplement. Deionized (DI) water ($\geq 18 \, M\Omega \, cm^{-1}$) was used in all experiments.

2.1 Aqueous photoreactor

The photoreactor is described in more detail in our previous study (Witkowski et al., 2019). The reaction vessel was a jacketed, quartz flask with an internal volume of 0.1 L. Radicals (OH) were generated in situ by photolyzing hydrogen peroxide (H_2O_2). The reaction vessel was surrounded by eight lamps (TUV TL 4W, Philips, $\lambda_{max} = 254 \, nm$). In some experiments, an ozone-free, 53.8 mm pen-ray lamp (11SC-2.12-PO-16-800, Analytik Jena, $\lambda_{max} = 254 \, nm$) was used. The pen-ray lamp was immersed in the reaction solution inside a quartz vial. Temperatures of the reaction solution were adjusted with a circulating water bath (SC100-A10, Thermo Fisher Scientific). The solution temperature was additionally monitored with an externally calibrated sensor (TP-361, Czaki Thermo-Product).

2.2 Chromatographic analyses

Semi-quantitative analyses of AAs were carried out with gas chromatography (GC) coupled with the flame ionization detector (FID) or with mass spectrometry (MS).

GC/MS analyses were carried out using a GC/MS-QP2010 Ultra (Shimadzu) gas chromatograph coupled with a single-quadrupole mass spectrometer equipped with an electron ionization (70 eV) ion source. The instrument was equipped with an AOC-5000 autosampler (Shimadzu). Analytes were separated with a VF-WAXms column (Agilent) or with a ZB-5MSplus column (Phenomenex) – Sect. S2.1. The mass spectrometer was operating in the selected ion monitoring mode (Tables S1 and S2).

GC/FID analyses were carried out using a GC17A gas chromatograph (Shimadzu). Analytes were separated with a ZB-Waxplus capillary column (Phenomenex). The GC/FID instrument was used for the analysis of C_5–C_{10} AAs, as well as for the C_2–C_4 linear AAs (Tables S3 and S4).

2.3 Experimental procedures

AAs under investigation were separated into four groups, based on their OH reactivities, chromatographic peak shape on a given stationary phase, GC detector response, and recoveries obtained following liquid–liquid extraction of aqueous samples taken from the photoreactor with ethyl acetate (Tables S1–4).

The concentration of cyclic, terpenoic, and C_5–C_{10} AAs (Tables S1, S2, and S4) in the reaction solution was 0.2–0.4 mM each, and the concentration of H_2O_2 was 0.1 M. The concentration of C_2–C_4 AAs (Table S3) in the reaction solution was 0.8–1.0 mM each, and the concentration of H_2O_2 in these experiments was 0.4 M.

AAs under investigation were first dissolved in water, and the resulting solution was filtered through a 0.7 µm glass fiber (GF) syringe filter and transferred to the reaction vessel. The temperature of the solution was allowed to stabilize before adding H_2O_2, which initiated the reaction.

Thirteen aliquots were sampled from the reaction solution, and the reaction time was 15–70 min, depending on the temperature and concentration of H_2O_2. The C_2–C_4 AAs (Table S3) were analyzed by injecting 0.5 µL of the aqueous sample taken from the reactor into the GC/FID instrument. For the rest of the AAs under investigation, 800 µL of the reaction solution was saturated with NaCl and extracted with 300 µL of ethyl acetate containing 0.3 mM of dimethyl phthalate (internal standard). Afterward, the organic layer was dried with anhydrous sodium sulfate (Na_2SO_4) and analyzed with the GC/MS or GC/FID instrument.

2.4 Relative rate technique and activation parameters

The $k_{OH_{aq}}$ values for the AAs under investigation were derived with Eq. (1).

$$Ln\left(\frac{[AA]_0}{[AA]_t}\right) = \frac{k_{AA}}{k_{Ref}} Ln\left(\frac{[Ref]_0}{[Ref]_t}\right) \quad (1)$$

In Eq. (1), [AA] and [Ref] are the initial (0) and intermediate concentrations of the AAs under investigation and the kinetic reference compound, respectively. k_{Ref} and k_{AA} ($M^{-1} s^{-1}$) are the $k_{OH_{aq}}$ for the kinetic reference compound and the AAs under investigation at a given temperature, respectively. 1,4-Butanediol and 1,5-pentanediol – $k_{OH_{aq}}$ at 298 K = $(3.5 \pm 0.1) \times 10^9 \, M^{-1} \, s^{-1}$ and $(4.4 \pm 0.7) \times 10^9 \, M^{-1} \, s^{-1}$, respectively – were used as the primary kinetic reference compounds (Hoffmann et al., 2009).

The temperature-dependent $k_{OH_{aq}}$ values were used to obtain the pre-exponential factors (A) and activation energies (E_a) using the Arrhenius expression (Eq. 2).

$$\mathrm{Ln}\left(k_{OH_{aq}}\right) = \mathrm{Ln}(A) - \left(\frac{E_a}{R}\right) \cdot \frac{1}{T} \qquad (2)$$

In Eq. (2), $k_{OH_{aq}}$ is the bimolecular reaction rate coefficient of the reaction of AAs with the OH ($\mathrm{M^{-1}\,s^{-1}}$) at a given temperature, T is the temperature (K), R is the gas constant ($\mathrm{kJ\,K^{-1}\,mol^{-1}}$), A is the pre-exponential factor ($\mathrm{M^{-1}\,s^{-1}}$), and E_a is the activation energy ($\mathrm{kJ\,mol^{-1}}$). The values of Gibbs free energy of activation ($\Delta G^{\ddagger}$), the enthalpy of activation ($\Delta H^{\ddagger}$), and the entropy of activation ($\Delta S^{\ddagger}$) were also calculated for each AA, using the temperature-dependent $k_{OH_{aq}}$ values (Sect. S4). The rates of diffusion-limited reactions (k_{diff}, $\mathrm{M^{-1}\,s^{-1}}$) were calculated with the Smoluchowski equation (Sect. S5) (Schöne et al., 2014; Krofliè et al., 2020).

2.5 Structure–activity relationship

The SAR methodology used in this work was introduced by Atkinson (1987) and later used to develop SAR for estimating the values of $k_{OH_{aq}}$ of aliphatic molecules containing C, H, and O atoms (Monod and Doussin, 2008; Doussin and Monod, 2013). SAR parameters include F and G substituent factors for CH_3, CH_2, CH, C, OH, FC=O, COOH, and COO– moieties; F factors for the C_6, C_5, and C_4 rings; and base rate coefficients for the H-atom abstraction from CH_3, CH_2, CH, and –OH groups (Fig. 1).

The partial rate coefficients are modified by the functional groups in the α and β positions using the F and G substituent factors (Monod and Doussin, 2008; Doussin and Monod, 2013). Note that fenchol has two fused C_5 rings and one C_6 ring, and the partial k values for H-atom abstraction connected with these rings are adjusted with the $F(C_5)$ and $F(C_6)$ factors (Fig. 1a; Monod and Doussin, 2008). Furthermore, in this work, an additional F factor was introduced (Sect. 3.2) for the H atoms connected with a straight-chain carbon backbone $\geq C_6$ (Fig. 1b).

A dataset containing the values of $k_{OH_{aq}}$ (298 K) for 56 AAs, carboxylic acids, and carboxylate anions (Witkowski, 2023) was used to derive the values of F and G factors by minimizing values of the Q parameter (Eq. 3) using the Excel Solver routine (González-Sánchez et al., 2021).

$$Q = \sum_n \frac{\left(k_{SAR} - k_{exp}\right)^2}{\sigma_n^2} \qquad (3)$$

In Eq. (3), k_{SAR} and k_{exp} are estimated and measured $k_{OH_{aq}}$ values at 298 K, and σ is the experimental uncertainty.

The temperature dependence of the partial k_{OH} values for CH_3, CH_2, CH, and OH groups is described via Eq. (4) using C and D factors. (Kwok and Atkinson, 1995) C and D factors

(a)

1) $\mathbf{k(CH)} \times F(OH)_9 \times F(C)_{10} \times F(C)_{11} \times G(CH_3)_2 \times G(CH_3)_3 \times G(CH_3)_7 \times G(CH)_4 \times G(CH_2)_6 \times G(CH_2)_8 \times F(C_6) \times F(C_5)$
2) $\mathbf{k(CH)} \times F(C)_{10} \times G(CH_3)_3 \times G(CH)_4 \times G(CH)_1$
3) $\mathbf{k(CH_3)} \times F(C)_{10} \times G(CH_3)_2 \times G(CH)_4 \times G(CH)_1$
4) $\mathbf{k(CH)} \times F(CH_2)_5 \times F(CH_2)_8 \times F(C)_{10} \times G(CH_2)_6 \times G(C)_{11} \times G(CH)_1 \times G(CH_3)_2 \times G(CH_3)_3 \times F(C_6) \times F(C_5)$
5) $\mathbf{k(CH_2)} \times F(CH_2)_6 \times F(CH)_4 \times G(C)_{10} \times G(CH_2)_8 \times G(C)_{11} \times F(C_6) \times F(C_5)$
6) $\mathbf{k(CH_2)} \times F(C)_{11} \times F(CH_2)_5 \times G(CH_3)_7 \times G(CH_2)_8 \times G(CH)_1 \times G(CH)_4 \times F(C_6) \times F(C_5)$
7) $\mathbf{k(CH_3)} \times F(C)_{11} \times G(CH)_1 \times G(CH_2)_6 \times G(CH_2)_8$
8) $\mathbf{k(CH_2)} \times F(CH)_4 \times F(C)_{11} \times G(C)_{10} \times G(CH_2)_5 \times G(CH)_1 \times G(CH_3)_7 \times G(CH_2)_6 \times F(C_5) \times F(C_5)$
9) $\mathbf{k(OH)} \times F(CH)_1 \times G(C)_{10} \times G(C)_{11}$

$k_{OH}(\text{Fenchol}) = \sum_{n=1}^{9}(k_n(\text{adjusted partial rate coefficients})$

(b)

1) $\mathbf{k(CH_2)} \times F(OH)_8 \times F(CH_2)_2 \times G(CH_3)_3 \times F_{((CH_2)_6)}$
2) $\mathbf{k(CH_2)} \times F(CH_2)_1 \times F(CH_2)_3 \times G(OH)_8 \times G(CH_2)_4 \times F_{((CH_2)_6)}$
3) $\mathbf{k(CH_2)} \times F(CH_2)_2 \times F(CH_2)_4 \times G(CH_2)_1 \times G(CH_2)_5 \times F_{((CH_2)_6)}$
4) $\mathbf{k(CH_2)} \times F(CH_2)_3 \times F(CH_2)_3 \times G(CH_2)_2 \times G(CH_2)_6 \times F_{((CH_2)_6)}$
5) $\mathbf{k(CH_2)} \times F(CH_2)_6 \times F(CH_2)_4 \times G(CH_2)_7 \times G(CH_2)_3 \times F_{((CH_2)_6)}$
6) $\mathbf{k(CH_2)} \times F(CH_2)_5 \times F(CH_2)_7 \times G(CH_2)_4 \times F_{((CH_2)_6)}$
7) $\mathbf{k(CH_3)} \times F(CH_2)_6 \times G(CH_2)_5 \times F_{((CH_2)_6)}$
8) $\mathbf{k(OH)} \times F(CH_2)_1 \times G(CH_2)_2$

$k_{OH}(\text{1-Heptanol}) = \sum_{n=1}^{8}(k_n(\text{adjusted partial rate coefficients})$

Figure 1. Examples of estimating the values of $k_{OH_{aq}}$ with SAR for fenchol (**a**) and 1-heptanol (**b**).

in Eq. (4) were adjusted using a database of 351 temperature-dependent rate coefficients (Witkowski, 2023).

$$k_{OH_{partial}}(T) = CT^2 \times \exp\left(\frac{-D}{T}\right) \qquad (4)$$

In Eq. (4), T is the reaction temperature (K). Furthermore, the values of F and G factors were adjusted at different temperatures with Eq. (5).

$$F \text{ or } G(T) = \exp\left(\frac{298 \times \ln(F \text{ or } G \text{ at } 298\,K)}{T}\right) \qquad (5)$$

After adjusting the values of the neighboring parameters (F and G), they were kept unchanged, and the values of D and C factors (Eq. 4) were adjusted with the measured, temperature-dependent $k_{OH_{aq}}$ values for AAs (this work) and for carboxylic acids and carboxylate (di)anions (Witkowski, 2023).

2.6 Control measurements and uncertainty

The reported uncertainties of the $k_{OH_{aq}}$ values measured in this work were derived with the exact differential method

(Eq. 4), taking into account the uncertainties of the slopes of kinetic plots (Eq. 1) and the uncertainties of the k_{ref} values reported in the literature (Schöne et al., 2014) – see Sect. S6 for a detailed derivation of this formula.

$$\Delta k_{OH_{aq}} = \sqrt{(\text{slope} \times \Delta k_{ref})^2 + (k_{ref} \times \Delta \text{slope})^2} \quad (6)$$

In Eq. (4), the slope is the slope of the kinetic plot corresponding to the k_{AA}/k_{ref} ratio (Eq. 1); Δslope is the experimental uncertainty, which was derived as 2σ from three or more separate measurements; and k_{ref} and Δk_{ref} are the $k_{OH_{aq}}$ values for the kinetic reference compounds and their uncertainties, respectively (Hoffmann et al., 2009). Uncertainties of the E_a values are reported as standard errors of the linear fitting (Eq. 2), and the uncertainties for the other activation parameters (Eqs. S1–3) were calculated with the exact differential method. Control experiments carried out without turning on the lamp or without adding H_2O_2 to the reaction solution confirmed that the AAs under investigation did not undergo direct photolysis or dark reactions with the H_2O_2 within the timescale of the experiments. To further confirm that the five terpenoic alcohols and diols under investigation were photochemically stable under the experimental conditions used, their UV–Vis spectra were acquired (Fig. S5). Also, no evaporation of the analytes was observed within the studied temperature range (Sect. 2.1). Control experiments also confirmed that the AAs that were analyzed in the same batch (Sect. S3) were not converted into one another during $R(I)$.

3 Results and discussion

3.1 Results of the kinetic measurements

The unknown $k_{OH_{aq}}$ values were calculated using Eq. (1); for all experiments, the squared linear coefficients of determination (R^2) > 0.99 were obtained, as shown in the representative relative kinetic plots (Fig. 2).

The values of $k_{OH_{aq}}$ measured in the temperature range between 278 and 323 K were used to calculate activation parameters. For all AAs under investigation, linear Arrhenius plots (Eq. 2) were obtained, as shown by the representative data presented in Fig. 3.

The $k_{OH_{aq}}$ values measured at 298 K and the activation parameters for the AAs investigated in this work are listed in Table 1; all temperature-dependent $k_{OH_{aq}}$ values measured in this work are listed in Table S6.

The majority of the $k_{OH_{aq}}$ values measured in this are work in very good agreement with the literature data, within the uncertainties reported (Table 1), thereby confirming that the experimental approach used in this work is reliable. To date, only one measured $k_{OH_{aq}}$ value is available for 1-hexanol, 1-heptanol, 1-octanol, 1,2-butanediol, and 1,6-hexanediol (Scholes and Willson, 1967; Hoffmann et al., 2009; Anbar et al., 1966), and the preferred values are based only on these single measurements (Table 1). For this reason, uncertainties of

33 % were recommended for the $k_{OH_{aq}}$ values for these five AAs (IUPAC, 2019). At the same time, the $k_{OH_{aq}}$ values measured in this work for 1-hexanol, 1-heptanol, 1-octanol, 1,2-butanediol, and 1,6-hexanediol are in good agreement with the preferred values, within the reported (and recommended) uncertainties.

For 1-propanol and 1- and 2-butanols, the values of $k_{OH_{aq}}$ measured in this work are noticeably lower than the preferred values (Table 1). However, these differences are difficult to explain. In the case of ethanol, 1,2-propanediol, 1,2-ethanediol, and 1,2-butanediol, for which the values of $k_{OH_{aq}}$ were measured together with 1-propanol and 1- and 2-butanols (Table S2), using the same kinetic reference compound (1,4-butanediol), an excellent agreement with the previously measured values was obtained (Table 1 – see also Fig. 4). One possible explanation may be that product peaks overlapped with the chromatographic peaks corresponding to AAs under investigation, which would lower the rate of disappearance of 1-propanol and 1- and 2-butanols during $R(I)$ obtained from the GC/FID measurements. This would result in the lower $k_{OH_{aq}}$ measured for these three AAs. To test that hypothesis, additional experiments were carried out by adding only 1-propanol, 1- and 2-butanols, and ethanol to the reaction solution to minimize the possible interferences from the products. The $k_{OH_{aq}}$ values obtained from these additional measurements for 1-propanol and 1- and 2-butanols were the same (within the obtained uncertainties – Table S8) as those reported in Table 1.

To our knowledge, for the rest of the AAs investigated in this work, including C_9–C_{10} n-alcohols, C_7–C_{10} α,ω-diols, and cyclic AAs and diols, the $k_{OH_{aq}}$ values were measured for the first time. The data obtained for these compounds are discussed in more detail later in this section.

The data acquired in this work and the literature data showed an incremental increase in the measured $k_{OH_{aq}}$ values in the homolog series of n-alcohols and α,ω-diols, which exhibited a distinctive curvature around four or five carbon atoms (Fig. 4a and b). In Fig. 5a, the preferred $k_{OH_{aq}}$ values (when available) for the AAs investigated in this work are superimposed with the data for n-alkanes. Very similar curvature was observed in the gas phase for the homolog series of n-alcohols (Fig. 5b; Mellouki et al., 2003; Monod et al., 2005).

In the gas phase, the curvature in Fig. 5b was attributed to the long-range activating effect of the –OH moieties, which extends to around four carbon atoms (Mellouki et al., 2003). This activating effect of –OH is due to the formation of a hydrogen-bonded (H-bonded) complex between OH and some oxygenated organics. The curving (Fig. 5b) is observed because the H-atom abstraction proceeds via a cyclic transition state (TS), which becomes less energetically favorable for the longer-chain molecules (Smith and Ravishankara, 2002). This mechanism is also confirmed by the limited data available for diols; the $k_{OH_{gas}}$ values for 1,2-ethanediol, 1,4-butanediol, 1,3-butanediol, 1,2-butanediol,
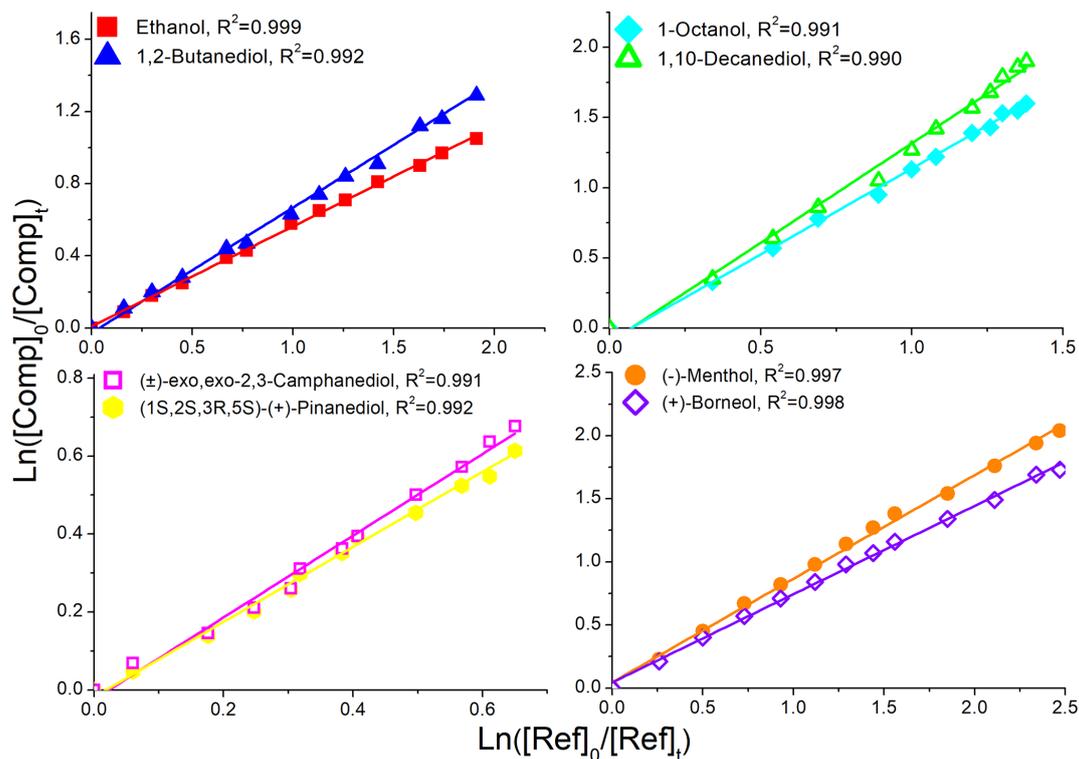
Figure 2. Sample relative kinetic plots obtained in this work at 298 K; data are represented by points, and lines are linear fits to the experimental data.
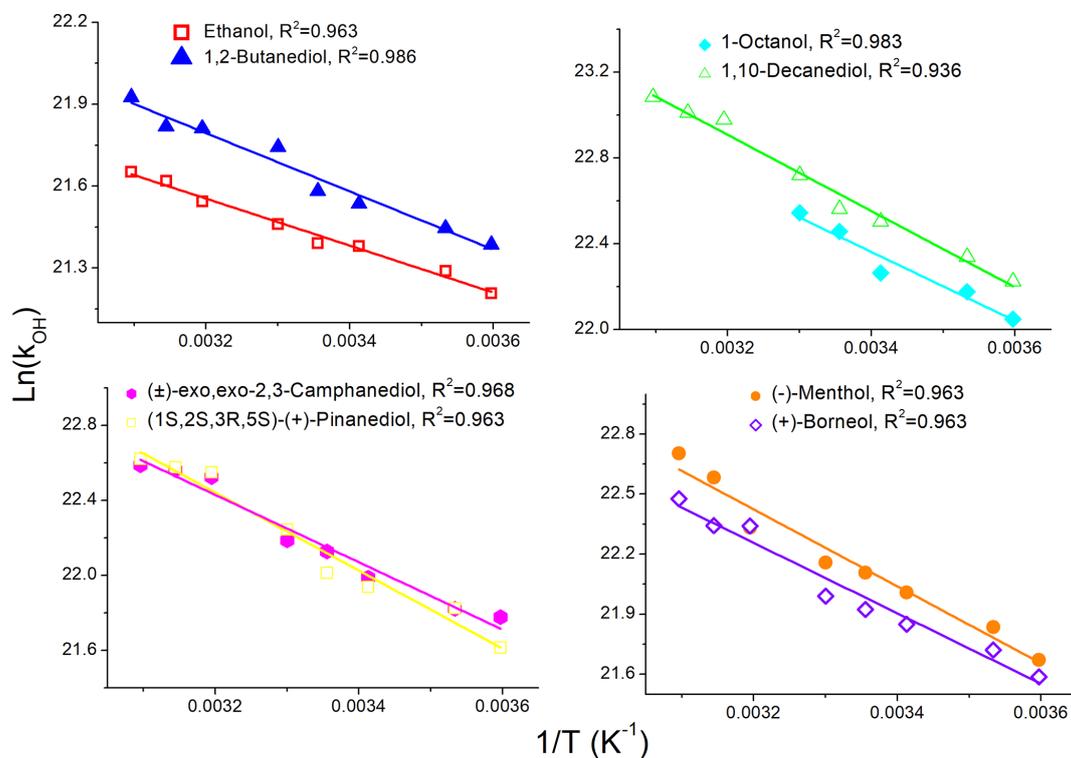
Figure 3. Sample Arrhenius plots obtained in this work; data are represented by points, and lines are linear fits to the experimental data.
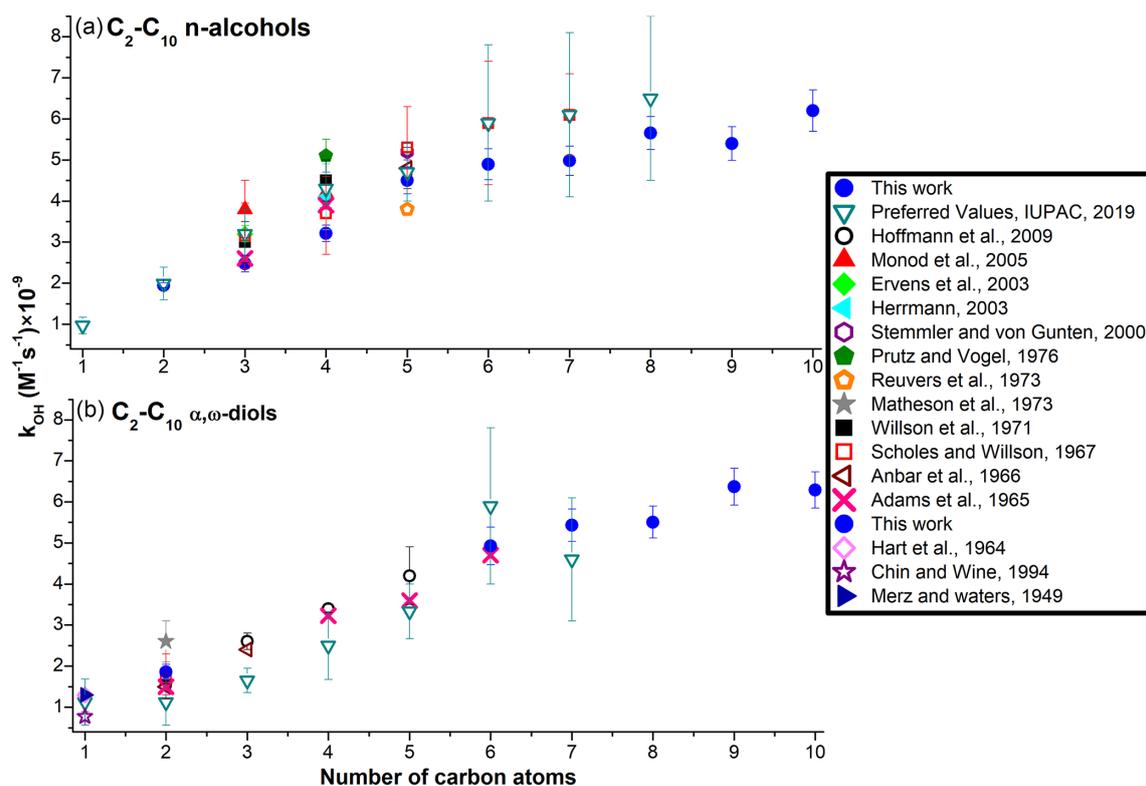
Figure 4. The $k_{OH_{aq}}$ values measured at 298 K for the homolog series of n-alcohols (**a**) and α,ω-diols (**b**). For the C_6–C_8 n-alcohols and 1,6-hexanediol, the preferred values are based on a single, measured $k_{OH_{aq}}$ value, with a recommended uncertainty of 33 %. For methanediol (formaldehyde hydrate), measured $k_{OH_{aq}}$ values from Merz and Waters (1947), Hart et al. (1964), and Chin and Wine (1994) are included.

and 2,3-butanediol are significantly higher compared to the corresponding n-alcohols and n-alkanes (Fig. 5b) (McGillen et al., 2021).

However, in the aqueous phase, the formation of this H-bonded complex is suppressed, most likely due to the H bonds between the water molecules and the –OH moieties of AAs (Monod et al., 2005). The suppression of the formation of the H-bonded complex between OH and –OH moieties explains the lack of the activating effects of one or two –OH moieties in the aqueous phase; the values of $k_{OH_{aq}}$ are the same for C_1–C_7 n-alkanes, n-alcohols, and α,ω-diols (Fig. 5a). At the same time, the assumption that in the aqueous phase n-alcohols and α,ω-diols react via the same mechanism as n-alkanes (direct abstraction of aliphatic H atoms by the OH) (Monod et al., 2005) does not explain the curvatures observed in Fig. 4a and b.

In the aqueous solutions, it was proposed that abstraction of aliphatic H atoms by the OH proceeds via a highly polarized (and possibly ionized) TS, which is stabilized by water molecules via polar interactions or the formation of H bonds (Mitroka et al., 2010). However, the electronegative moieties (here –OH) compete for electron density with OH, thereby lowering the stabilization of this polar TS by the water molecules. For the lower-molecular-weight (MW) AAs (and ethers) this effect is largely offset by the resonance

stabilization of the TS (Mitroka et al., 2010), which likely becomes less important for the longer-chain molecules. These assumptions would explain the lower $k_{OH_{aq}}$ measured for the C_5–C_{10} n-alcohols and α,ω-diols (curving of the plot in Fig. 5a) compared to the corresponding n-alkanes.

The new kinetic data acquired in this work (Table 1) also indicate that the curving observed in the aqueous phase (Fig. 5a) is somewhat suppressed at higher temperatures for n-alcohols and especially for α,ω-diols (Fig. S6); naturally, diols can form a higher number of H bonds with water than n-alcohols. Consequently, it is reasonable to assume that hydrophobic interactions (HIs) can contribute to this phenomenon, including the formation of hydration spheres around the alkyl chains (Otto and Engberts, 2003). The H-atom transfer from organic reactants to OH is largely influenced by the number of water molecules (and the strength of H bonds between them) in the first hydration shell (Krofliè et al., 2020; Yamabe and Yamazaki, 2018). At the same time, the stability of H bonds between the water molecules in the hydration shell is decreased at higher temperatures (Chandler, 2005; Ross and Rekharsky, 1996; Otto and Engberts, 2003). For the longer-chain AAs, with larger hydration shells, weakening of the H bonds between the water molecules and between water and –OH moieties (at $T > 298$ K) may render the aliphatic H atoms more suscep-
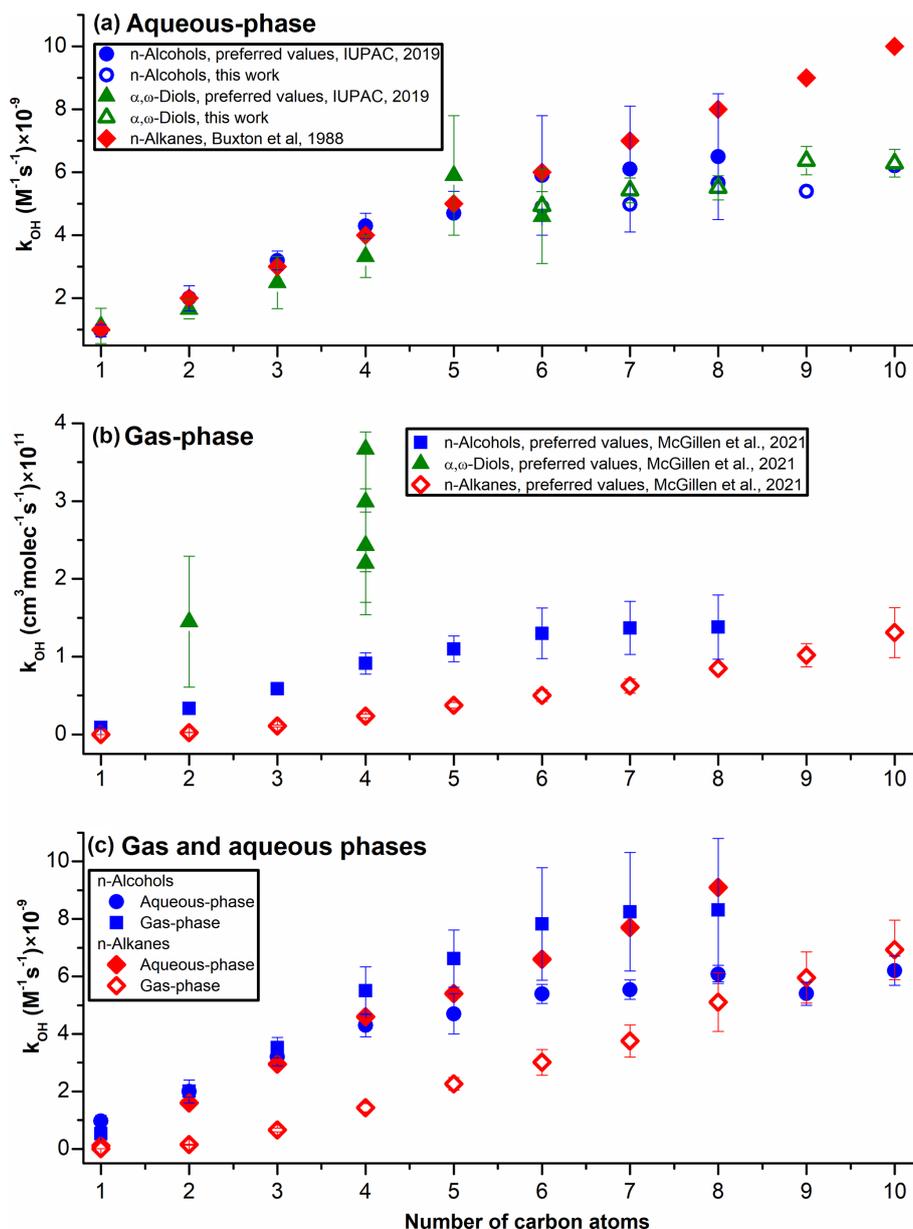
Figure 5. Measured k_{OH} values for *n*-alkanes, *n*-alcohols, and diols in the gas (a) and aqueous (b) phases. When available, preferred (recommended) values are shown for both phases (see also Table S5). (a) For the 1-hexanol, 1-heptanol, 1-octanol, 1,2-butanediol, and 1,6-hexanediol, the preferred values are based on single measurements; hence for these AAs, the values of $k_{OH_{aq}}$ measured in this work are also included. (b) The preferred values are shown, when available, and diols were not included due to the very low number of $k_{OH_{aq}}$ values available to date. (c) For C_6–C_{10} *n*-alcohols, average values (preferred values and data acquired in this work) are shown, and the uncertainties shown were obtained with the error propagation method. (a, c) No $k_{OH_{gas}}$ values are currently available for *n*-decanol and 1-nonanol. (a, c) For the C_1–C_{10} *n*-alkanes, the majority of $k_{OH_{aq}}$ values are based on single measurements (Table S5), and no preferred values (or their uncertainties) are currently available.

tible to abstraction by the OH. Naturally, in water, *n*-alkanes are also surrounded by H-bonded hydration layers, but the presence of –OH moieties can alter the hydration shells for the entire molecules (here AAs), which can explain the differences in the $k_{OH_{aq}}$ values for the C_6–C_{10} *n*-alkanes, *n*-alcohols, and α,ω-diols (Fig. 5c; Otto and Engberts, 2003).

Furthermore, when the $k_{OH_{aq}}$ and of $k_{OH_{gas}}$ values are compared directly, for the $> C_5$ molecules, *n*-alkanes undergo faster oxidation in water compared to *n*-alcohols, whereas the opposite trend is observed in the gas phase for all C_1–C_{10} homologs (Fig. 5c). In both gas and aqueous phases, OH most likely reacts with *n*-alkanes via the direct H-atom ab-

Table 1. The values of $k_{OH_{aq}}$ obtained in this work for the reaction of OH with AAs at 298 K, literature data, and the preferred values.

| Compound | k_{OH} at 298 K, $(M^{-1} s^{-1}) \times 10^{-9}$ | | |
	This work	Literature[a]	Reference
Ethanol[b]	2.0 ± 0.1	2.0 ± 0.4	IUPAC (2019)
1-Propanol	2.5 ± 0.2	3.2 ± 0.6	IUPAC (2019)
		3.8 ± 0.7	Monod et al. (2005)
		3.2 ± 0.2	Ervens et al. (2003)
		3.0 ± 0.5	Willson et al. (1971)
		3.2 ± 0.8	Scholes and Willson (1967)
		2.6	Adams et al. (1965)
1-Butanol	3.2 ± 0.2	4.3 ± 0.4	IUPAC (2019)
		4.1 ± 0.8	Herrmann (2003)
		4.2 ± 0.4	Monod et al. (2005)
		4.5 ± 0.5	Willson et al. (1971)
		5.1 ± 0.4	Prutz and Vogel (1976)
		3.7 ± 1	Scholes and Willson (1967)
		3.9	Adams et al. (1965)
2-Butanol	2.5 ± 0.2	3.2 ± 0.3	IUPAC (2019)
		3.5 ± 0.4	Herrmann (2003)
		2.8 ± 0.7	Scholes and Willson (1967)
		3.1	Adams et al. (1965)
		2.4 ± 0.2	Anbar et al. (1966)
1-Pentanol	4.5 ± 0.3	4.7 ± 0.7	IUPAC (2019)
		5.1 ± 0.2	Stemmler and von Gunten (2000)
		3.8	Reuvers et al. (1973)
		5.3 ± 1	Scholes and Willson (1967)
		4.8 ± 0.5	Anbar et al. (1966)
1-Hexanol	4.9 ± 0.4	5.9 ± 1.9	IUPAC (2019)
		5.9 ± 1.5	Scholes and Willson (1967)
1-Heptanol	5.0 ± 0.4	6.1 ± 2	IUPAC (2019)
		6.1 ± 1	Scholes and Willson (1967)
1-Octanol	5.7 ± 0.4	6.5 ± 2	IUPAC (2019)
		6.5 ± 2	Scholes and Willson (1967)
1-Nonanol	5.4 ± 0.4		
1-Decanol	6.2 ± 0.5		
3-Ethyl-3-pentanol	2.5 ± 0.3		
1,2-Ethanediol	1.9 ± 0.2	1.7 ± 0.3	IUPAC (2019)
		1.6 ± 0.03	Hoffmann et al. (2009)
		2.6 ± 0.5	Matheson et al. (1973)
		1.62	Willson et al. (1971)
		1.8 ± 0.5	Scholes and Willson (1967)
		1.5 ± 0.3	Anbar et al. (1966)
		1.5 ± 0.2	Adams et al. (1965)
1,2-Propanediol	1.8 ± 0.1	1.75 ± 0.6	IUPAC (2019)
		1.6 ± 0.3	Hoffmann et al. (2009)
		1.7	Adams et al. (1965)
		1.7 ± 0.4	Scholes and Willson (1967)

Table 1. Continued.

| Compound | k_{OH} at 298 K, $(M^{-1} s^{-1}) \times 10^{-9}$ | | |
	This work	Literature[a]	Reference
1,2-Butanediol	2.4 ± 0.2	2.2 ± 0.4	IUPAC (2019)
		2.2 ± 0.4	Hoffmann et al. (2009)
1,6-Hexanediol	4.9 ± 0.4	4.6 ± 1.5	IUPAC (2019)
		4.7	Anbar et al. (1966)
1,7-Heptanediol	5.4 ± 0.4		
1,8-Octanediol	5.5 ± 0.4		
1,9-Nonanediol	6.4 ± 0.4		
1,10-Decanediol	6.3 ± 0.4		
Cyclohexanol	3.6 ± 0.3		
trans-1,2-Cyclohexanediol	2.9 ± 0.1		
exo-Norborneol	1.9 ± 0.1		
cis-2-Methylcyclohexanol	4.8 ± 0.5		
(+)-Fenchol	3.0 ± 0.2		
(+)-Borneol	3.3 ± 0.1		
(−)-Menthol	4.0 ± 0.1		
(±)-*exo,exo*-2,3-Camphanediol	4.1 ± 0.1		
(1S,2S,3R,5S)-(+)-Pinanediol	3.6 ± 0.1		

[a] Preferred values are based on the data compiled by the IUPAC Task Group on Atmospheric Chemical Kinetic Data Evaluation. Note also that for relative measurements, a large number of the $k_{OH_{aq}}$ values listed in the original studies reviewed by the task group were recalculated using the updated k_{ref} values for the kinetic reference compounds. [b] For clarity, only the preferred value is given for ethanol, due to a very large number of measured $k_{OH_{aq}}$ values for these two AAs. Note that the preferred values given in the IUPAC data sheets and their uncertainties reflect both the distribution and number of the previously measured $k_{OH_{aq}}$ values.

straction (Monod et al., 2005). In water, the resulting (highly polar) TS is stabilized by the solvent, which contributes to the higher k_{OH} values for *n*-alkanes (Fig. 5c). However, for *n*-alcohols (Fig. 5c), the formation of the less energetically favorable TS (no H-bonded complex) in water most likely contributes to the observed decrease in the k_{OH} values for the C$_4$–C$_{10}$ molecules. Also, for the lower-MW *n*-alcohols, the formation of the less energetically favorable TS in water may be partially offset by its resonance stabilization. Moreover, HIs can also contribute to the observed decrease in the k_{OH} values for AAs in the aqueous phase compared to the gas phase (Fig. 5c).

The conclusions presented in this section indicate that, in the case of aliphatic, oxygenated molecules, the rates of $R(I)$ in water may be largely influenced by the solvent effects: HIs and H-bond formation. More often than not, such solvent effects will offset the direct activating effects of the oxygenated moieties, especially for the longer-chain molecules. However, further studies, likely involving computational methods, are needed to provide more quantitative conclusions.

The temperature-dependent values of $k_{OH_{aq}}$ measured in this work were used to derive activation parameters for the AAs under investigation (Table 2).

The values of E_a obtained in this work for all AAs are much higher (Table 2) than the values for the same reactions in the gas phase, which also indicates a different, higher-energy TS in the aqueous phase (Mellouki et al., 2003; Monod et al., 2005). In the homolog series of *n*-alcohols and α,ω-diols, the values of E_a increased (Fig. 6a and e), before reaching the average value of approximately 15 (kJ × mol^{-1}). Similar E_a values were obtained for the nine cyclic AAs under investigation (Table 2). In addition to HIs (already discussed in this section), an increasing diffusion contribution (Table S3) can also contribute to the higher E_a values for the longer-chain AAs (Sarang et al., 2021; Schöne et al., 2014). In solution, the rate of reaction is diffusion-limited if every encounter between reactants (here AAs and OH) leads to a reaction (Sarang et al., 2021). Consequently, the E_a for the aqueous reactions with a high diffusion contribution is expected to approach 15 (kJ × mol^{-1}),

Table 2. The values of activation parameters obtained in this work.

Compound	$A \times 10^{-11}$ ($M^{-1} s^{-1}$)	E_a ($kJ\,mol^{-1}$)	$\Delta H^{\ddagger}$ ($kJ\,mol^{-1}$)	$\Delta S^{\ddagger}$ ($J\,mol^{-1} \times K$)	$\Delta G^{\ddagger}$ ($kJ\,mol^{-1}$)	R^{2*}
Ethanol	0.4 ± 0.05	7.1 ± 0.3	4.6 ± 0.3	$-(51.2 \pm 1.1)$	19.9 ± 0.5	0.984
1-Propanol	0.8 ± 0.1	8.5 ± 0.4	6.0 ± 0.4	$-(44.7 \pm 1.2)$	19.3 ± 0.5	0.989
2-Butanol	1.9 ± 0.3	10.6 ± 0.3	8.1 ± 0.3	$-(37.5 \pm 1.1)$	19.3 ± 0.5	0.994
1-Butanol	2.5 ± 0.3	10.7 ± 0.3	8.3 ± 0.3	$-(34.9 \pm 0.9)$	18.7 ± 0.4	0.995
1-Pentanol	6.2 ± 1.3	12.1 ± 0.5	9.7 ± 0.5	$-(27.4 \pm 1.8)$	17.8 ± 0.7	0.989
1-Hexanol	8.2 ± 2.6	12.6 ± 0.8	10.1 ± 0.8	$-(25.2 \pm 2.6)$	17.6 ± 1.1	0.978
1-Heptanol	14.4 ± 6.1	13.9 ± 1.1	11.4 ± 1.1	$-(20.5 \pm 3.5)$	17.5 ± 1.5	0.966
1-Octanol	26.6 ± 1.3	14.1 ± 2.0	11.6 ± 2	$-(19.4 \pm 6.8)$	17.4 ± 2.8	0.944
1-Nonanol	26.6 ± 2.1	15.1 ± 1.2	12.6 ± 3.2	$-(15.4 \pm 7.2)$	17.2 ± 1.6	0.968
1-Decanol	32.8 ± 2.6	15.6 ± 2.6	13.1 ± 2.6	$-(13.6 \pm 2.6)$	17.2 ± 2.6	0.987
3-Ethyl-3-pentanol	6.4 ± 2.1	13.8 ± 0.8	11.3 ± 0.8	$-(27.2 \pm 2.7)$	19.4 ± 1.2	0.979
1,2-Ethanediol	0.4 ± 0.1	7.8 ± 0.7	5.3 ± 0.7	$-(49.6 \pm 2.4)$	20.1 ± 1.0	0.951
1,2-Propanediol	0.5 ± 0.1	8.2 ± 0.6	5.7 ± 0.6	$-(48.6 \pm 2.2)$	20.2 ± 0.9	0.964
1,2-Butanediol	0.9 ± 0.2	8.8 ± 0.7	6.3 ± 0.7	$-(43.9 \pm 2.3)$	19.4 ± 1.0	0.966
1,6-Hexanediol	4.9 ± 1.6	11.3 ± 0.8	8.8 ± 0.8	$-(29.5 \pm 2.8)$	17.6 ± 1.2	0.968
1,7-Heptanediol	7.8 ± 2.8	12.2 ± 0.9	9.7 ± 0.9	$-(25.5 \pm 3.0)$	17.4 ± 1.3	0.969
1,8-Octanediol	31.8 ± 4.5	15.6 ± 1.1	13.2 ± 1.1	$-(13.9 \pm 3.8)$	17.3 ± 1.6	0.969
1,9-Nonanediol	14.8 ± 2.5	13.5 ± 0.4	11.0 ± 0.4	$-(20.2 \pm 1.4)$	17.0 ± 0.6	0.994
1,10-Decanediol	26.2 ± 7.6	14.8 ± 0.7	12.3 ± 0.7	$-(15.5 \pm 2.4)$	16.9 ± 1.0	0.986
Cyclohexanol	15.2 ± 6.0	14.8 ± 1.2	12.3 ± 1.2	$-(20.0 \pm 3.8)$	18.3 ± 1.6	0.965
trans-1,2-Cyclohexanediol	5.1 ± 2.0	12.7 ± 1.0	10.2 ± 1.0	$-(29.1 \pm 3.2)$	18.9 ± 1.4	0.966
exo-Norborneol	6.9 ± 2.0	14.5 ± 1.4	12.0 ± 1.4	$-(26.6 \pm 4.8)$	19.9 ± 2.0	0.943
cis-2-Methylcyclohexanol	18.4 ± 5.1	14.5 ± 1.4	12.1 ± 1.4	$-(18.4 \pm 4.1)$	17.5 ± 1.7	0.959
(+)-Fenchol	21.6 ± 7.9	16.3 ± 0.9	13.8 ± 0.9	$-(17.1 \pm 3.0)$	18.9 ± 1.3	0.982
(+)-Borneol	12.4 ± 3.5	14.5 ± 1.1	12.1 ± 1.1	$-(21.7 \pm 3.6)$	18.5 ± 1.5	0.967
(−)-Menthol	37.4 ± 4.8	16.9 ± 1.0	14.4 ± 1.0	$-(12.5 \pm 3.3)$	18.1 ± 1.4	0.980
(±)-*exo,exo*-2,3-Camphanediol	17.2 ± 5.1	14.9 ± 1.0	12.4 ± 1.0	$-(19.0 \pm 3.4)$	18.1 ± 1.4	0.972
(1S,2S,3R,5S)-(+)-Pinanediol	43.4 ± 10.1	17.3 ± 1.3	14.8 ± 1.3	$-(11.3 \pm 4.2)$	18.2 ± 1.8	0.966

* Squared coefficients of determination for the obtained Arrhenius plots.

likely due to the temperature dependence of the viscosity of water, which also follows the Arrhenius relationship (Ervens et al., 2003). For all AAs under investigation, positive $\Delta H^{\ddagger}$ values, between 4 and 15 ($kJ\,mol^{-1}$) were obtained. In the homolog series of n-alcohols and α,ω-diols, the values of $\Delta H^{\ddagger}$ (Fig. 6b and f) follow the incremental increase in the E_a values (Eq. S1); a similar increase in the values of $\Delta S^{\ddagger}$ was observed (Fig. 6c and g). For the majority of C_1–C_{10} AAs, the literature (preferred) values of activation parameters also follow the general trends observed in this work, with the largest discrepancies observed for C_2–C_4 n-alcohols (Fig. 6a–c) and 1,2-ethanediol (Fig. 6g–h). For 1-butanol the recommended values of activation parameters (Fig. 6a–d) are based on a single study, and the values derived in this work are closer to the data obtained by Herrmann (2003).

More experimental data are needed to provide a better estimate of the values of activation parameters for 1-butanol; analysis of the data available for 1,2-ethanediol (Fig. 6g–h) leads to a similar conclusion (Hoffmann et al., 2009).

Negative values of $\Delta S^{\ddagger}$ were obtained for all AAs under investigation (Table 2). Higher (less negative) values of $\Delta S^{\ddagger}$

were obtained for the higher-MW AAs (including also cyclic AAs – Table 2), corresponding to a smaller decrease in disorder following $R(I)$. Such a result may be associated with a release of water molecules from the hydrophobic surfaces (here alkyl chains) (Krofliè et al., 2020). As previously concluded, for some phenols, this phenomenon led to positive (or close to zero) values of $\Delta S^{\ddagger}$, even though the formation of a new bond between the reactants leads to a decrease in the disorder (Krofliè et al., 2020). The increase in the values of $\Delta S^{\ddagger}$ for the higher-MW AAs (with longer hydrophobic alkyl chains) also supports the assumption that the HIs influence the mechanism of $R(I)$. The $\Delta G^{\ddagger}$ values (this work and literature data) are very similar (within the uncertainties reported – Fig. 6d and h) since the values of $\Delta H^{\ddagger}$ and $\Delta S^{\ddagger}$ underwent similar incremental increases for all AAs under investigation (Eq. S3). Similar values of $\Delta G^{\ddagger}$ indicate the same TS and reaction mechanism (Ervens et al., 2003). The average $\Delta G^{\ddagger}$ of $18 \pm 2\,kJ\,mol^{-1}$ obtained in this work (Table 2) is close to the previously reported values for the reaction of OH with the oxygenated, aliphatic molecules (Schaefer et al., 2020; Ervens et al., 2003; Witkowski et al., 2021;
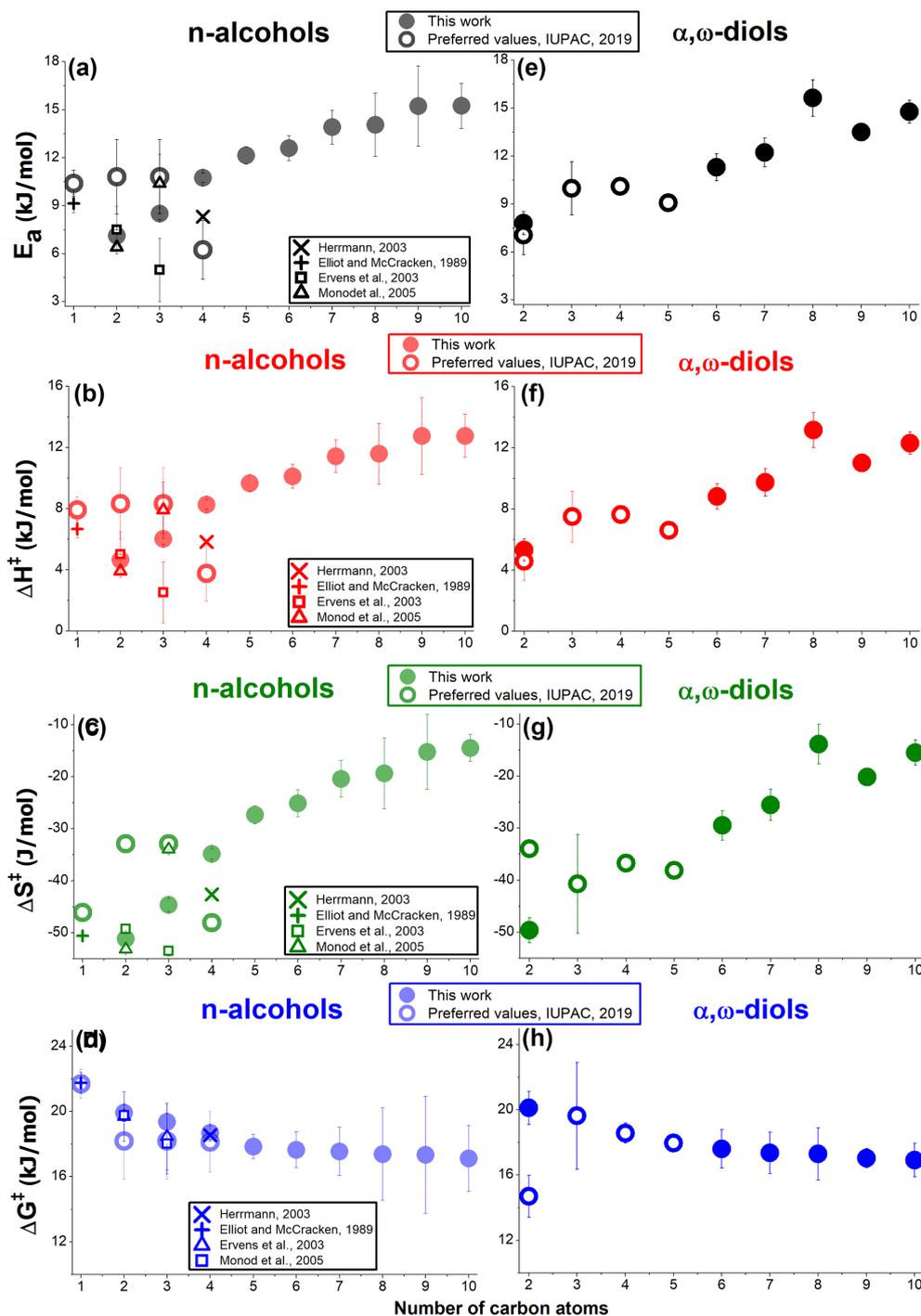
Figure 6. The values of activation parameters (derived in this work and literature values) for the homolog series of C_1–C_{10}, linear n-alcohols, and α,ω-diols. The literature data shown are based on the preferred values (IUPAC, 2019); no recommendations currently are available for methanediol (formaldehyde hydrate).

Hoffmann et al., 2009; Otto et al., 2018). Consequently, the values of activation parameters obtained in this work confirm a predominance of the H-atom abstraction mechanism (Witkowski et al., 2021; Ervens et al., 2003; Schaefer et al., 2020; Otto et al., 2018).

More patterns can be recognized by examining the k_{OH} values for the linear, cyclic, and poly-alcohols in both gas and aqueous phases. Some diols and poly-alcohols with –OH moieties separated by more than one carbon atom exhibit noticeably higher values of $k_{\mathrm{OH_{aq}}}$ compared to their vici-

nal analogs; this trend can be observed for the C_3–C_6 AAs (Fig. 7a–d) (IUPAC, 2019; Hoffmann et al., 2009). The preferred $k_{OH_{aq}}$ values for 1-propanol (Fig. 7a), 1-butanol (Fig. 7b), and 1-pentanol (Fig. 7c) also follow this general trend. At the same time, results are somewhat inconclusive when the preferred k_{OH} values for 1-hexanol and 1,6-hexanediol are considered, due to their relatively high uncertainties (Fig. 7d). In the gas phase, the $k_{OH_{gas}}$ values for the vicinal butanediols are lower compared to the 1,4-butanediol, but this conclusion is again somewhat implied by the statistical data (Fig. 7e). Generally, an insufficient number of the $k_{OH_{gas}}$ values are available for diols to present more definitive conclusions (McGillen et al., 2021).

Under the assumption that the trends illustrated in Fig. 7 are not related directly to the solvent effects (and hence are also observed in the gas phase – Fig. 7e), the lower k_{OH} values for the vicinal poly-alcohols and diols may be rationalized by considering their structural features. In 1,2-diols the –OH moieties most likely interact via polarization and electrostatic effects, rather than forming intramolecular hydrogen bonds (Das et al., 2015; Klein, 2003). Such interactions may affect the mesomeric donor effect of –OH (Monod and Doussin, 2008), thereby resulting in the observed decrease in the measured $k_{OH_{aq}}$ values for the vicinal poly-alcohols.

The experimental data acquired in this work and the literature data (McGillen et al., 2020; McGillen, 2021; Buxton et al., 1988) also revealed noticeably lower $k_{OH_{aq}}$ values for some cyclic AAs and hydrocarbons compared to their linear analogs (Fig. 8a–c). This trend is especially noticeable for *exo*-norborneol, which possesses a bridged cyclohexane ring (effectively two fused C_5 rings). Note, however, that the preferred $k_{OH_{aq}}$ values for C_6 and C_7 linear AAs and diols are the same as their cyclic analogs within the reported uncertainties (IUPAC, 2019).

For alkanes, the $k_{OH_{aq}}$ values are the same (within the uncertainties reported) for both cyclic and linear molecules (Fig. 8d). Furthermore, the $k_{OH_{gas}}$ values are the same for the *n*-hexane and cyclohexane (and also for the corresponding alcohols), within the uncertainties reported (Fig. 8e). Also, no uncertainty has been reported for the $k_{OH_{gas}}$ value for *n*-octane; for this reason, it is not possible to evaluate whether or not the $k_{OH_{gas}}$ value for *n*-octane differs significantly from ethylcyclohexane (Fig. 8e).

The lower $k_{OH_{aq}}$ values for some cyclic AAs may be caused by the different mobilities of the linear and cyclic reactants inside the water cage, resulting in a different intramolecular selectivity of OH (Kopinke and Georgi, 2017). However, more experimental data are needed to provide more insights into the reactivities of the aliphatic, oxygenated molecules containing aliphatic rings; for instance, the $k_{OH_{aq}}$ values measured in this work for *cis*-2-methylcyclohexanol, 1-heptanol, and 1,7-heptane diol are the same; the preferred $k_{OH_{aq}}$ values for the C_7 AAs also support this conclusion (Fig. 8b).

3.2 Structure–activity relationship

The $k_{OH_{aq}}$ values measured in this work at 298 K and the literature data (Sect. 2.5) were used to optimize F and G factors only for CH_2 and –OH moieties (Model 1) or substituent factors for CH_3, CH_2, CH, and –OH moieties; C_4–C_6 rings; and the base (partial) rate coefficients (Model 2; Table 3). Model 2 also included a new substituent factor for molecules with straight-chain carbon backbones – $F \geq (CH_2)_6$ (Fig. 1).

The unadjusted SAR included the neighboring parameters and partial rate coefficients originally derived by Monod and Doussin (2008) and Doussin and Monod (2013), as well as F and G factors for carboxylic acids and carboxylate ions recently updated by our group (Witkowski et al., 2021). Note also that *cis*-pinonic acid was the only carbonyl compound in the kinetic dataset used in this work to optimize SAR parameters (Witkowski, 2023). As demonstrated in our previous study, hydration (formation of gem-diol) of *cis*-pinonic acid is negligible (Witkowski et al., 2021).

In Table 3, the F and G values >1 indicate activation, whereas values <1 correspond to the deactivating effect of a given group (Kwok and Atkinson, 1995). The values of F and G factors are often rationalized via the field and resonance effects, which are expressed by the values of R (resonance) and F (field) parameters defined by Swain and Lupton (1968). The resonance effects primarily affect the α position, whereas the field effects are mostly associated with the β positions (Monod and Doussin, 2008). In Table 4, the negative values correspond to the electron-donating group (activating effect), whereas positive values indicate deactivation (electron withdrawing). Consequently, alkyl substituents should exhibit activating effects in both α and β position following their negative values of F and R parameters, whereas α activation and β deactivation are expected for –OH (Table 4).

In Model 1, the F and G factors of 1.40 (F) and 0.63 (G) for –CH_2 and 1.51 (F) and 0.81 (G) for –OH were obtained, which only resulted in a moderate improvement of the SAR accuracy (Fig. 9b), even though a majority of model compounds (Table 1) possessed both of these moieties, which should result in a reliable model fit (Peduzzi et al., 1996).

The values obtained for –OH (Model 1) are similar to the previously reported values (Monod and Doussin, 2008), but the strong β-deactivating effect of CH_2 (Fig. 9b) is difficult to rationalize in the context of the field and resonance effects for alkyl substituents (Table 4). Such behavior of Model 1 most likely reflects the trends in OH reactivities observed for the homolog series of linear alcohols and diols in the aqueous phase (Figs. 4 and 5).

By only adjusting the F and G factors for –OH and CH_2, it was impossible to further improve the performance of SAR. Moreover, the accuracy of Model 1 was higher for AAs but significantly lower for carboxylic acids and carboxylate ions (Fig. 9b). In an attempt to further improve the model, all substituent factors and partial rate coefficients were adjusted.
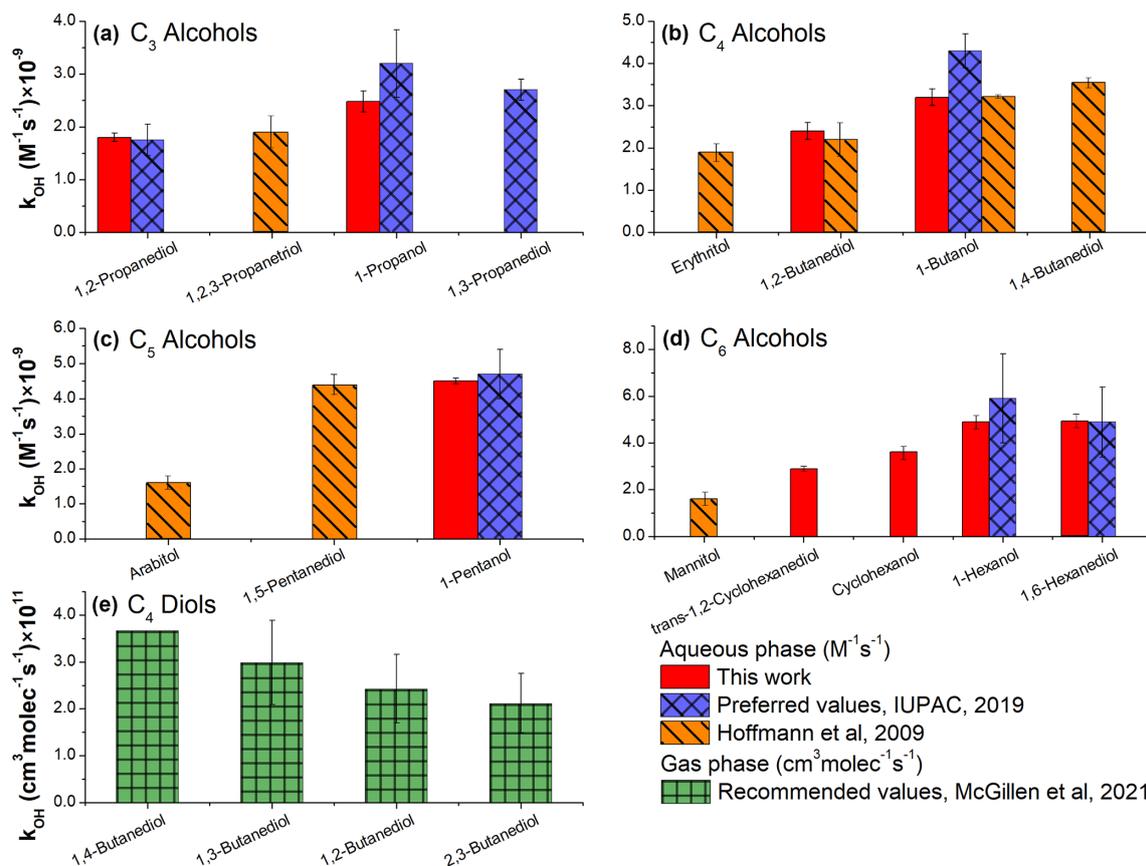
Figure 7. Measured k_{OH} values (this work and literature data) for the selected mono- and poly-alcohols. When available, the preferred (recommended) values are shown (IUPAC, 2019; McGillen, 2021). For the three sugar alcohols (erythritol, arabitol, mannitol), the data reported by Hoffmann et al. (2009) are presented.

The resulting SAR parameters showed very little correlation with the factors proposed by Swain and Lupton (results not shown). At the same time, only a minor improvement in the SAR performance was achieved, but the obtained G-parameter values for the CH_2 group were always <1.

The original SAR developed by Monod and Doussin was based on the values of $k_{OH_{aq}}$ measured primarily for the lower-MW molecules, which is reflected by the large positive bias of the unadjusted model (slope = 1.648, Fig. 9a), especially for the longer-chain AAs (Doussin and Monod, 2013; Monod and Doussin, 2008). Consequently, using this methodology, which was originally developed for predicting the values of $k_{OH_{gas}}$, an adequate representation of the aqueous OH reactivity of higher-MW molecules in the aqueous phase is difficult.

For this reason, it was concluded that there is a need for an additional parametrization of the observed reactivity of the WSOCs with larger carbon backbones (Fig. 5). Therefore, a new F factor, reflecting the reactivities of the longer-chain molecules, was introduced (Table 3). In Model 2, the partial k_{OH} of every CH_2 moiety is additionally adjusted for the C_6 and longer-chain precursors, which resulted in a noticeably

higher accuracy of SAR (Fig. 9c). Following this adjustment, the versatility and accuracy of Model 2 were noticeably improved, resulting in the better performance for alcohols, diols, and carboxylic acids and carboxylate anions (Fig. 9c). The accuracy of SAR (Model 2) was lowest for cyclic alcohols (Fig. 9b). The F factors <1 obtained for the C_5 and C_6 rings reflect the lower OH reactivates observed in this work for the cyclic AAs (Fig. 8).

In Model 2, the adjusted values of the neighboring parameters and partial rate coefficients for the alkyl groups (CH_3, CH_2, and CH; Table 3) are all in good agreement with the previously reported data (Monod and Doussin, 2008). Furthermore, the substituent factors derived for –OH are also in very good agreement with the literature data and correlate well with the resonance and field effects of the hydroxyl moiety (Table 4). The value of the partial rate coefficient for the abstraction of H atom from the –OH was approximately 3 times lower than the rates obtained for the CH_n groups (Table 2), thereby confirming that a direct abstraction of H atom from –OH is a minor reaction pathway (Monod and Doussin, 2008; Atkinson, 1986a; Kwok and Atkinson, 1995).
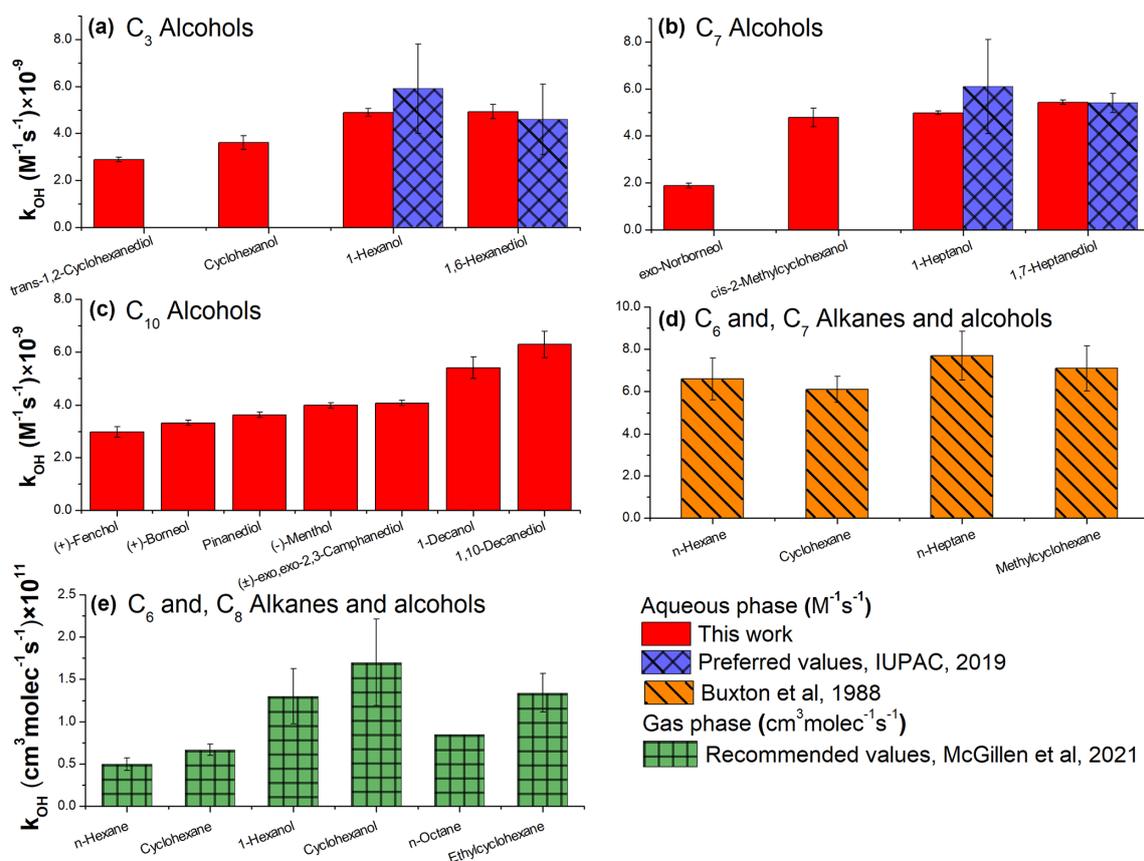
Figure 8. k_{OH} values at 298 K for the cyclic and linear alcohols and diols in the aqueous **(a–c)** and gas **(d, e)** phases. When available, the preferred (recommended) values are shown (IUPAC, 2019; McGillen, 2021). For the sugar alcohols, the data reported by Hoffmann et al. (2009) are presented. For 1-hexanol and 1,6-hexanediol **(a, b)** both the preferred values (IUPAC, 2019) and the data acquired in this work are included.

The optimized SAR (Model 2) was used to obtain the values of C and D factors (Eqs. 4 and 5), which allows for predicting the temperature-dependent $k_{OH_{aq}}$ values for AAs and carboxylic acids induced in the model training set (Fig. 10).

The overall performance of Model 2 was similar for alcohols and carboxylic acids under investigation, in the temperature range between 278–328 K; the best performance was obtained for 298 K, likely because the values of neighboring parameters were optimized using the values of $k_{OH_{aq}}$ measured at this temperature (Sect. 2.5 and Eq. 3). The values of squared coefficients of determination (R^2) and slopes obtained from the linear regression analysis for different groups of compounds (Fig. 10) are presented in Fig. 11 – these data are listed in Table S9.

The accuracy of Model 2 in the studied temperature range was satisfactory for AAs, diols, carboxylic acids, and carboxylate anions. The model showed a slight negative bias at temperatures >308 K for mono-alcohols (Fig. 11a), diols, and glycerine (Fig. 11b). Furthermore, the correlation between the measured and predicted $k_{OH_{aq}}$ values was lower for both higher and lower temperatures. This may be due to the non-linear effects of the temperature on the $k_{OH_{aq}}$ values

observed for the n-alcohols and α,ω-diols (Sect. 3.1). Similar performance of Model 2 was also obtained for carboxylic acids (Fig. 11d) and carboxylate anions (Fig. 11e), and the model performance was unsatisfactory for the cyclic AAs investigated in this work (Fig. 11c). However, it is important to note that in the entire temperature range investigated in this work, the vast majority of $k_{OH_{aq}}$ values for cyclic alcohols were predicted within a factor of 2.

4 Atmospheric implications

4.1 Lifetimes of terpenoic alcohols

The lifetimes for the five TAs investigated in this work were estimated with Eq. (7) (Sarang et al., 2021).

$$\tau = \frac{1}{\left(\frac{k_{OH_{gas}}}{H_{OH}^{cc}} + k_{OH_{aq}} H_{AA}^{cc} \omega \right) [OH]_{aq}} \tag{7}$$

In Eq. (7), τ is the combined lifetime in the gas and the aqueous phase due to the reaction with the OH. Therefore, this approach considers both gas and aqueous oxidation of AAs by

Table 3. SAR (Model 2) substituent factors and base rate coefficients.

Group	Substituent factors		Reference
	F	G	
CH_3	1.40	1.16	This work
CH_2	1.34	1.00	This work
CH	1.03	1.05	This work
$\geq (CH_2)_6$	0.76		This work
C	1.00	1.00	Monod and Doussin (2008)
OH	1.97	0.56	This work
C_6	0.65		This work
C_5	0.61		This work
C_4	1.34		This work
$FC = O$	0.20	0.90	Doussin and Monod (2013)
COOH	0.16	0.59	Witkowski et al. (2021)
COO–	0.54	0.64	Witkowski et al. (2021)

Base (partial) rate coefficients, (k_{OH}) at 298 K $\times 10^{-8}$		
k_{CH_3}	4.06	
k_{CH_2}	6.17	This work
k_{CH}	4.40	
k_{OH}	1.54	

Temperature dependence of the base rate coefficients		
	$C \times 10^{-3}$, $(M^{-1}\,s^{-1})$	$D \times 10^{-2}$, (K)
k_{CH_3}	5.50	0.55
k_{CH_2}	197.9	9.98
k_{CH}	5.04	0.05
k_{OH}	1.74	0.01

(The "This work" label spans the temperature dependence rows.)

Table 4. Selected resonance (R) and field (F) factors; negative values correspond to activating effects and positive values indicate deactivation.

Group	Resonance effects (R, α position)	Field effects (F, β position)
–OH	−1.89	0.46
CH_3	−0.41	−0.1
$CH_3\,CH_2$	−0.44	−0.2

the OH and their relative importance, depending on Henry's law equilibria and LWC of a given air mass (Sarang et al., 2021).

In Eq. (7), $k_{OH_{gas}}$ and $k_{OH_{aq}}$ are the bimolecular reaction rate coefficients for the reaction of a given AA in the gas and aqueous phase with the OH ($M^{-1}\,s^{-1}$) at 298 K respectively. H_{OH}^{cc} and H_{AA}^{cc} are the dimensionless Henry's law constants for the OH (H_{OH}^{cc}) and for the given AA (H_{AA}^{cc}) (Sander, 2015), ω is the LWC ($m^3\,m^{-3}$), and $[OH]_{aq}$ is the aqueous concentration of OH (M). The gas-phase OH concentration is connected with $[OH]_{aq}$ via Henry's equilibrium, assuming that there are no additional sources of OH; the average reported $H_{OH}^{cc} = 764$ was used (Sander, 2015).

The $k_{OH_{aq}}$ values measured in this work were used to calculate the τ for the five TAs. For pinanediol, the $k_{OH_{gas}}$ value was predicted with SAR due to a lack of measured values. Likewise, when possible, the experimentally measured $k_{OH_{gas}}$ and H_{AA}^{cc} values were used; otherwise, the values listed were estimated with the structure–activity relationship (SAR) (Kwok and Atkinson, 1995; Atkinson, 1986b) and with HenryWin (Table 5).

The τ values were calculated as a function of LWC and $[OH]_{aq}$; the dotted lines in Fig. 12 represent the range of OH concentrations in different types of aqueous particles (Herrmann et al., 2010). The y axis (Fig. 12) represents the total lifetime (τ, h). The plateau regions, corresponding to the lower values of LWC, indicate that the reaction with the OH takes place only in the gas phase.

When this simplified model (Eq. 7) is used, the timescales of interactions of gaseous species (air masses) also have to be considered. An average, weighted residence time of an air parcel inside a cloud was estimated as approximately 3 h; by taking into account the total lifetime of a typical air parcel (~ 5 d), it will spend a total of 18 h inside a cloud (Herrmann et al., 2015). Furthermore, the aqueous-phase processing of organic molecules (here TAs) in the atmosphere is in-
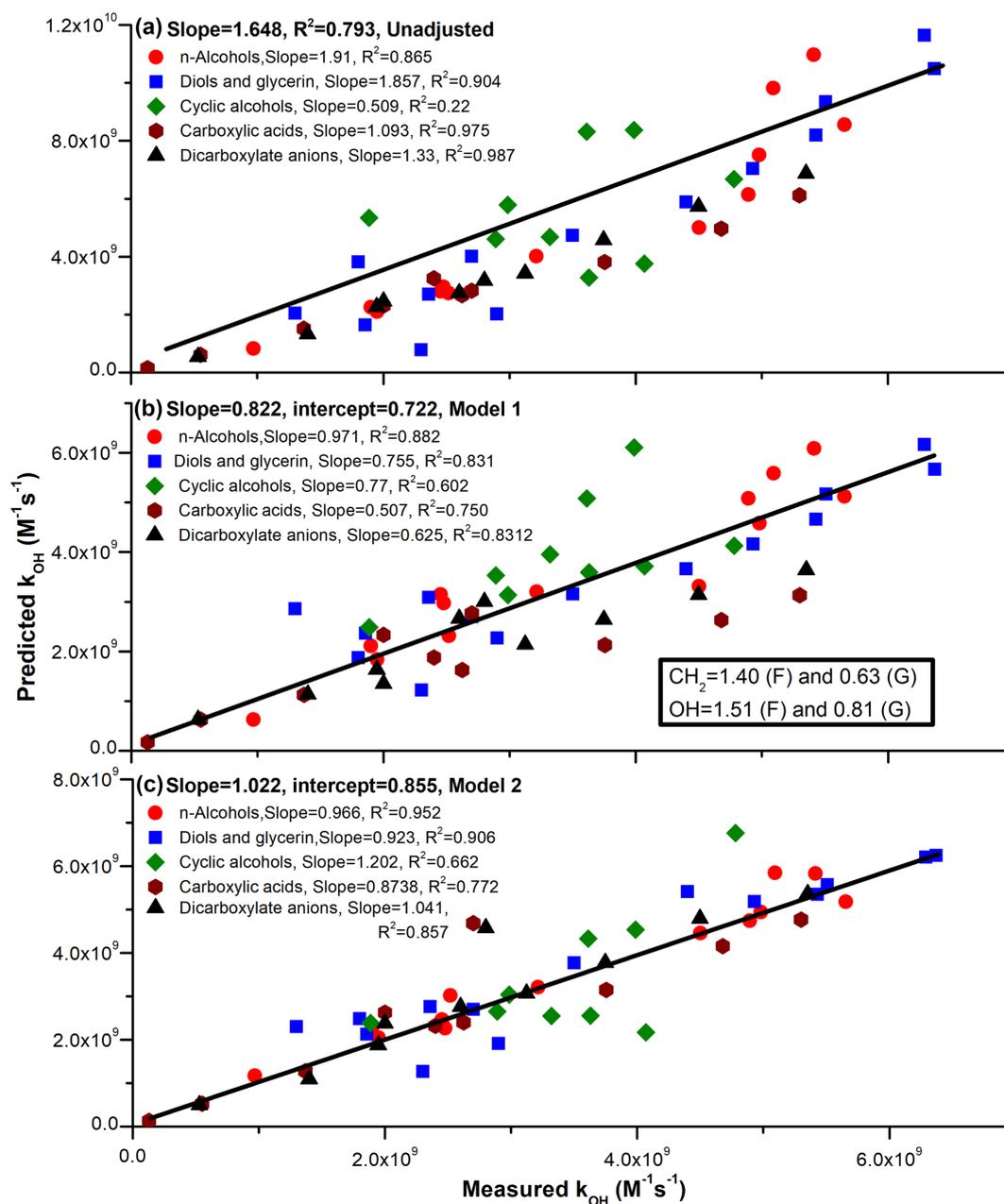
Figure 9. Accuracies of unadjusted (**a**) and adjusted (**b**, Model 1; **c**, Model 2) SARs for alcohols and carboxylic acids at 298 K.

terrupted by the evaporation of cloud and fog droplets, which occurs on a timescale of a few minutes (Ervens, 2015).

The new $k_{OH_{aq}}$ values acquired in this work indicate that TAs are likely to undergo aqueous oxidation in clouds with LWC $\geq 0.1\,\mathrm{g\,m^{-3}}$ (Fig. 12a–c), whereas terpenoic diols will react with the OH in aqueous aerosols, clouds, and fogs with LWC $\geq 10^{-4}\,\mathrm{g\,m^{-3}}$ (Fig. 9d–e). Considering the timescale of air-parcel interactions with clouds and fogs and the lifetimes of aqueous particles, all TAs under investigation can undergo $R(I)$ in maritime clouds (Fig. 12). At the same time, aqueous oxidation of TAs over the ocean is only plausible

at the ocean side (Hiura et al., 2021), whereas in marine aerosols, the dominant AAs are fatty and sugar alcohols (Fu et al., 2013). Only terpenoic diols can undergo $R(I)$ in both continental (here urban and remote) and marine clouds, with estimated lifetimes <1 min – well below the estimated lifetimes of cloud and fog droplets (Fig. 12d and e).

The aqueous oxidation of terpenoic acids by OH has received considerable attention in connection with the formation of $_{aq}$SOAs (Zhao et al., 2017; Amorim et al., 2020; Aljawhary et al., 2016; Otto et al., 2018; Amorim et al., 2021; Witkowski et al., 2018b, 2021; Witkowski and Gier-
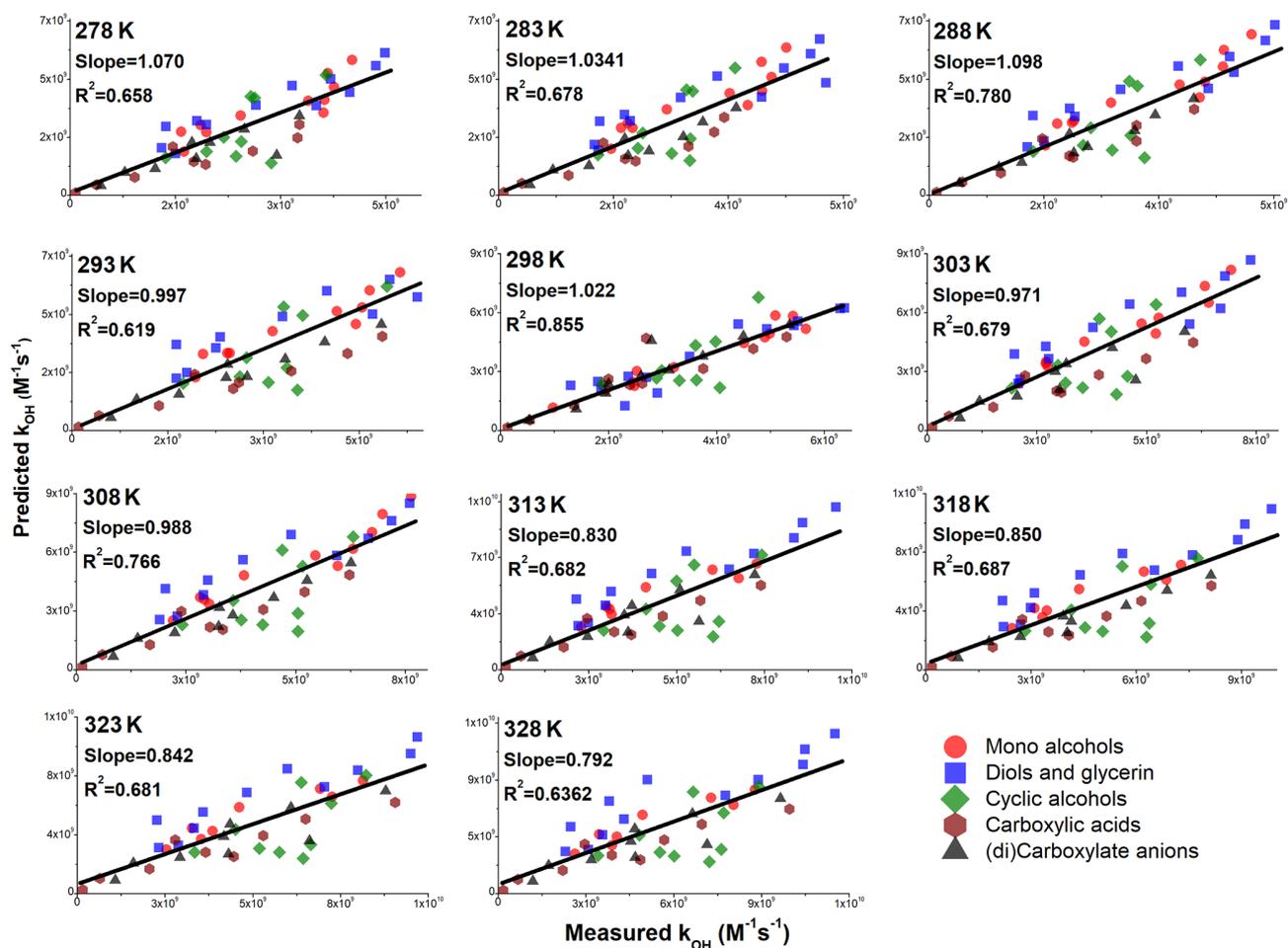
Figure 10. Accuracies of Model 2 for alcohols and carboxylic acids in the temperature range between 278 and 328 K. If for a given temperature the measured value of $k_{OH_{aq}}$ was not available, it was derived using the reported (or measured in this work) values of E_a and A – see also Appendix 1.

Table 5. Data used to estimate the atmospheric lifetimes of the five terpenoic alcohols due to reaction with the OH at 298 K.

Name	$k_{OH_{aq}} \times 10^{-9}$ $(M^{-1} s^{-1})$*	$k_{OH_g} \times 10^{11}$ $(cm^3$ molec.$^{-1} s^{-1})$	Reference	H^{cc}	Reference
Fenchol	2.99	2.49	McGillen et al. (2020), McGillen et al. (2021)	5.0×10^3	Fichan et al. (1999)
Borneol	3.32	2.65		5.08×10^3	Sander (2015)
Menthol	3.99	1.48		1.20×10^3	Sander (2015)
Camphanediol	4.07	2.78	Kwok and Atkinson (1995),	1.0×10^5	EPI Suite™ (2023)
Pinanediol	3.63	2.12	Atkinson (1986b)	1.0×10^5	

* $k_{OH_{aq}}$ values measured in his work.

czak, 2017; Witkowski et al., 2018a, 2019). Using the same approach (Eq. 7) we have recently derived τ values for six terpenoic acids, identified as the major components of unaged α-pinene SOA (Witkowski et al., 2023). In our previous work, it was concluded that when a given air mass is characterized by the LWC $\geq 1 \times 10^{-3}$ g m^{-3}, cis-pinic, cis-pinonic,

hydroxypinonic, and oxopinonic acids will react with the OH primarily in the aqueous phase (Witkowski et al., 2023). Hence, in the case of terpenoic diols (Fig. 12), their potential to undergo aqueous oxidation under realistic atmospheric conditions is comparable with some terpenoic acids. In the case of cis-pinonic acid, the measured mass yields of $_{aq}$SOAs
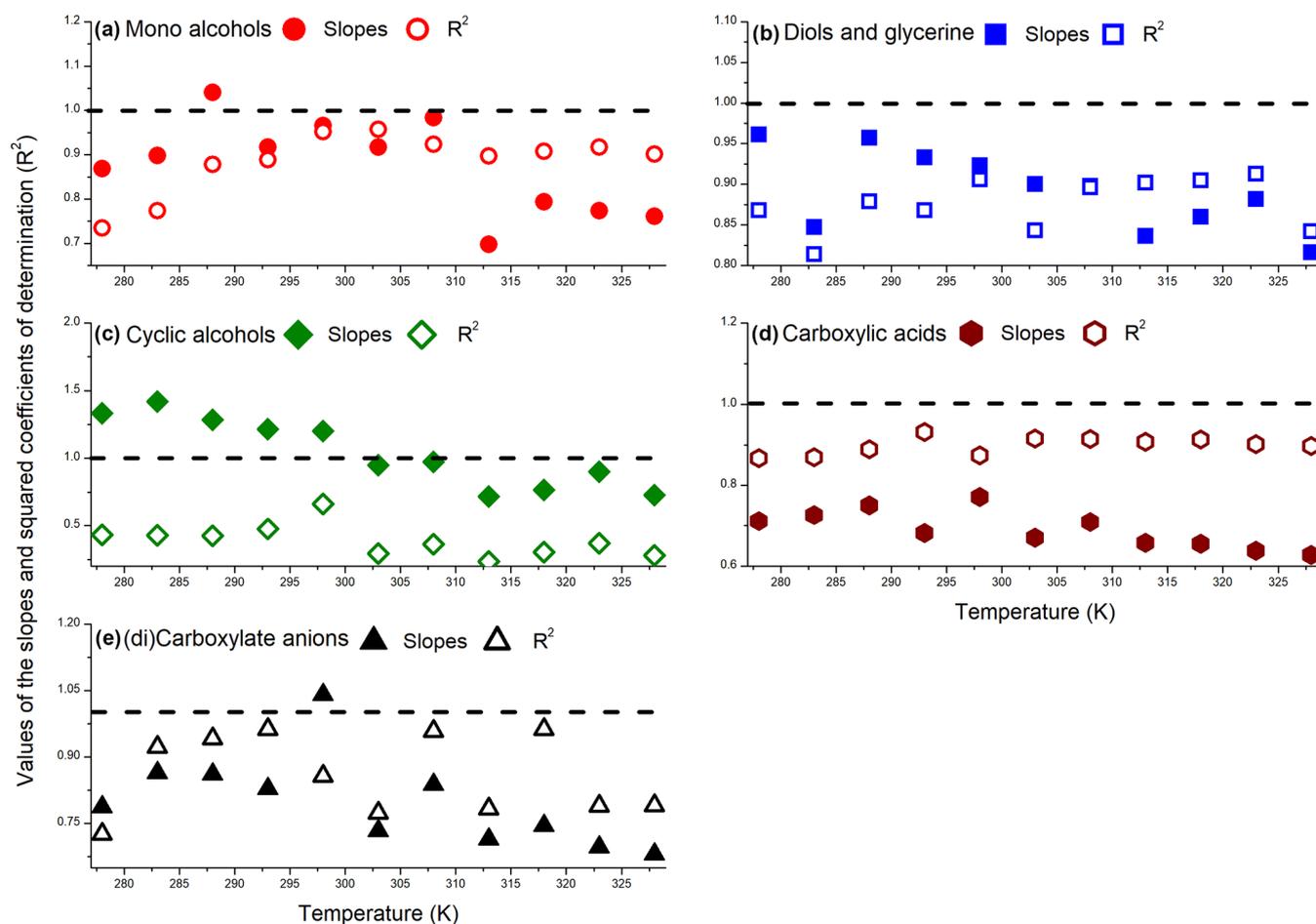
Figure 11. The values of slopes and squared coefficients of determination (R^2) obtained from the linear regression analysis of the performance of Model 2 for mono-alcohols **(a)**, diols and glycerine **(b)**, cyclic alcohols **(c)**, carboxylic acids **(d)**, and carboxylate anions **(e)** in the temperature range between 278–328 K. The dotted horizontal lines represent an ideal SAR model, which would have both slope and $R^2 = 1$.

following the reaction with the OH were as high as 60 %. (Al-jawhary et al., 2016) At the same time, to date, few mechanistic data are available about the formation of low-volatility products from TAs following $R(I)$.

Global emissions of oxygenated terpenes are tentatively estimated at $26 \, \mathrm{Tg \, C \, yr^{-1}}$ (teragrams of carbon per year) (Sindelarova et al., 2014). TAs are emitted by vegetation (Héral et al., 2021) but are also used in the industry as fragrance agents and solvents (Belsito et al., 2008). Therefore, TAs and especially terpenoic diols are potentially important precursors of $_{\mathrm{aq}}$SOAs in both urban and remote environments.

4.2 Influence of the temperature

The values of H^{cc}, $k_{\mathrm{OH_{aq}}}$, and $k_{\mathrm{OH_{gas}}}$ all depend on the temperature. In a relatively narrow temperature range in which liquid water exists in the atmosphere, the enthalpy of dissolution $\left(\frac{\mathrm{d ln}(H)}{\mathrm{d} 1/T} \right)$ can be considered constant. Hence, the Van 't Hoff equation can be applied to describe the temperature de-

pendence of H^{cc} values (Sander, 2015). For instance, a decrease in the temperature by 20° will result in a 2 to 7-fold increase in the H^{cc} values of TAs and OH (Sander, 2015). Consequently, a significantly higher fraction of these reactants will reside in the aqueous phase at lower temperatures, thereby strongly favoring the aqueous chemical aging of TAs in the atmosphere.

The data acquired in this work and the literature data confirm that the temperature dependence of the $k_{\mathrm{OH_{aq}}}$ values for the TAs follows the Arrhenius relationship (Witkowski, 2023). Considering the temperature range in which liquid water exists in the atmosphere, the same conclusion also applies to the temperature dependence of the $k_{\mathrm{OH_{gas}}}$ values for TAs and similar molecules. Furthermore, the values of E_a and A (Sect. 2.4) measured in this work, as well as literature data, show relatively similar temperature dependencies of $k_{\mathrm{OH_{aq}}}$ and $k_{\mathrm{OH_{gas}}}$ (Kwok and Atkinson, 1995; Atkinson, 1986a; McGillen et al., 2020; Hoffmann et al., 2009; Herrmann, 2003). Hence, the $k_{\mathrm{OH_{aq}}}/k_{\mathrm{OH_{gas}}}$ ratio for the TAs (Table 5) will remain mostly unchanged in the considered tem-
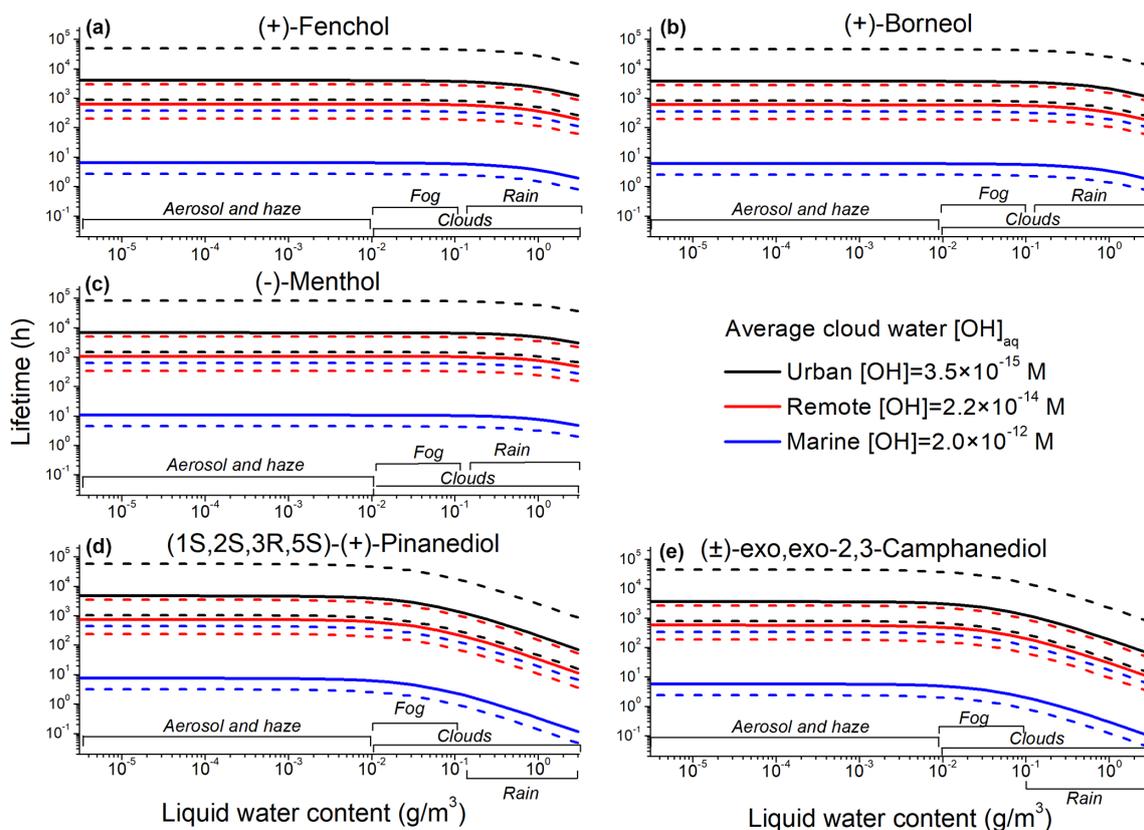
Figure 12. The estimated lifetimes of TAs. The dotted lines represent lifetimes corresponding to the minimum and maximum $[OH]_{aq}$ in different aqueous particles.

perature range. At the same time, a lower temperature will result in a lower oxidation rate, thereby decreasing the τ values, which can make other removal mechanisms more relevant.

These conclusions are valid primarily for cloud water droplets which are diluted and, more often than not, can be treated as ideal solutions (Richters et al., 2015; Herrmann, 2003). On the other hand, the ionic strength (I) of some aerosols can be as high as 43 (M) (Cheng et al., 2016). The high I values of some aerosols will affect the kinetics of $R(I)$, partitioning, and rates of diffusion of the reactants (Mekic and Gligorovski, 2021). While salting out of organics will likely occur in aqueous particles with high I value, salts are also expected to enhance the rate of $R(I)$ (Zhou et al., 2019).

4.3 Potential formation of $_{aq}$SOAs from terpenoic alcohols

No product studies were carried out in this work. Nevertheless, as indicated by the new kinetic data acquired in this work, the cyclic TAs investigated should be considered as the potential precursors of $_{aq}$SOAs. For instance, cyclic terpenes are often more efficient at forming SOAs compared to linear precursors (Hunter et al., 2014; Lim and Ziemann, 2009). Following $R(I)$, oxygenated functional groups are added to

the original carbon backbone of the precursor, according to Russell's and Bennett–Summers' mechanisms (Bennett and Summers, 1974; Russell, 1957). Alkoxy (RO) radicals are formed from the reaction of an alkyl radical with O_2 via the decomposition of tetroxide intermediates (von Sonntag and Schuchmann, 1991; Bennett and Summers, 1974). At the same time, in the case of linear precursors, the β-scission reaction of RO radicals can result in a decreased length of the carbon backbone (Enami and Sakamoto, 2016; Murakami and Ishida, 2017; Rauk et al., 2003). Consequently, β scission involving non-cyclic precursors results in lower MW and more volatile products that are less likely to contribute to SOAs (Enami and Sakamoto, 2016; Murakami and Ishida, 2017; Rauk et al., 2003). Hence, the cyclic precursors, such as TAs, are more likely to yield highly oxidized, low-volatility products following reaction with the OH without undergoing too much fragmentation (Ceacero-Vega et al., 2012; Claeys et al., 2009; Sato et al., 2016).

5 Conclusions and further work

The use of a bulk photoreactor combined with the offline, semi-quantitative analysis of the reacting WSOCs via gas chromatography allowed us to obtain $k_{OH_{aq}}$ for multiple com-

pounds from a single experiment (Herrmann et al., 2005; Monod et al., 2005). This method is significantly less laborious than some of the other methods of measuring $k_{OH_{aq}}$ and can be used to obtain large kinetic datasets, thereby facilitating the expansion of the aqueous kinetic databases for the environmentally widespread WSOCs.

The measured $k_{OH_{aq}}$ values for AAs (this work and literature data) revealed that it was necessary to introduce an additional neighboring parameter for the linear, longer-chain ($\geq C_6$) molecules to further improve the performance of the predictive model. The need to modify the methodology used in the original SAR was most likely connected with a different TS formed between OH and AAs in the gas and the aqueous phases (Mellouki et al., 2003; Herrmann et al., 2005; Smith and Ravishankara, 2002). It is still unclear if the new, modified SAR is capable of accurately predicting the values of $k_{OH_{aq}}$ for different oxygenated molecules, including carbonyls, esters, linear acids, and multifunctional molecules, possessing larger carbon backbones. More kinetic data for such molecules, including polyfunctional compounds, are needed to further improve the capabilities of kinetic predictive models (SARs).

Models utilized for generating explicit oxidation schemes of atmospherically abundant organics frequently rely on kinetic SARs to derive rate coefficients and branching ratios of the numerous by-products involved in a given mechanism (Bräuer et al., 2019). Hence, expanding the applicability domains of the aqueous kinetic SARs will further improve our ability to predict the effects of various, multiphase processes (such as formation and aging of $_{aq}$SOAs) on air quality, climate, and public health. Likewise, the dependence of the $k_{OH_{aq}}$ values from I also needs to be further investigated to provide insights into the timescales of $R(I)$ and other radical reactions in the presence of high amounts of salts (Herrmann et al., 2015).

The values of neighboring parameters in SAR for strained and non-strained rings remain somewhat ambiguous, again due to the very limited number of experimentally measured $k_{OH_{aq}}$ values for such molecules. Overall, the updated SAR (Model 2) showed good accuracy in the temperature range between 278–328 K, which also underlines the need to further expand the kinetic databases to include a larger number of the temperature-dependent $k_{OH_{aq}}$ values.

The atmospheric lifetimes estimated for the five TAs – fenchol, borneol, menthol, camphanediol, and pinanediol – underlined the need to further investigate other non-acidic precursors of $_{aq}$SOAs in the atmosphere. Recently, in connection with the formation of $_{aq}$SOAs, a lot of attention has been dedicated to studying acidic precursors, such as terpenoic acids. Higher-MW organic acids are expected to reside almost entirely in the aqueous phase, even at relatively low values of LWC. Likewise, all TAs, and especially diols, studied in this work can undergo $R(I)$ in clouds, fogs, and wet aerosols under realistic atmospheric conditions, which underlines the

need to study the formation of low-volatility products from such precursors.

Author contributions. BaW: conceptualization, supervision, original draft, data curation, methodology, and writing (review and editing). PJ: investigation, formal analysis, methodology, validation, data curation, and writing (review and editing). BeW: methodology and resources. TG: project administration, supervision, funding acquisition, resources, and writing (review and editing).

Competing interests. The contact author has declared that none of the authors has any competing interests.

Disclaimer. Publisher's note: Copernicus Publications remains neutral with regard to jurisdictional claims made in the text, published maps, institutional affiliations, or any other geographical representation in this paper. While Copernicus Publications makes every effort to include appropriate place names, the final responsibility lies with the authors.

Review statement. This paper was edited by Allan Bertram and reviewed by two anonymous referees.

References

Adams, G. E., Boag, J. W., and Michael, B. D.: Reactions of the hydroxyl radical, Part 2 – Determination of

absolute rate constants, T. Faraday Soc., 61, 1417–1424, https://doi.org/10.1039/TF9656101417, 1965.

Aljawhary, D., Zhao, R., Lee, A. K. Y., Wang, C., and Abbatt, J. P. D.: Kinetics, Mechanism, and Secondary Organic Aerosol Yield of Aqueous Phase Photo-oxidation of α-Pinene Oxidation Products, J. Phys. Chem. A, 120, 1395–1407, https://doi.org/10.1021/acs.jpca.5b06237, 2016.

Amorim, J. V., Wu, S., Klimchuk, K., Lau, C., Williams, F. J., Huang, Y., and Zhao, R.: pH Dependence of the OH Reactivity of Organic Acids in the Aqueous Phase, Environ. Sci. Technol., 54, 12484–12492, https://doi.org/10.1021/acs.est.0c03331, 2020.

Amorim, J. V., Guo, X., Gautam, T., Fang, R., Fotang, C., Williams, F. J., and Zhao, R.: Photo-oxidation of pinic acid in the aqueous phase: a mechanistic investigation under acidic and basic pH conditions, Environ. Sci.-Atmos., 1, 276–287, https://doi.org/10.1039/D1EA00031D, 2021.

Anbar, M., Meyerstein, D., and Neta, P.: Reactivity of aliphatic compounds towards hydroxyl radicals, J. Chem. Soc. B., 742–747, https://doi.org/10.1039/J29660000742, 1966.

Atkinson, R.: Estimations of OH radical rate constants from H-atom abstraction from CH and OH bonds over the temperature range 250–1000 K, Int. J. Chem. Kinet., 18, 555–568, https://doi.org/10.1002/kin.550180506, 1986a.

Atkinson, R.: Kinetics and mechanisms of the gas-phase reactions of the hydroxyl radical with organic compounds under atmospheric conditions, Chem. Rev., 86, 69–201, https://doi.org/10.1021/cr00071a004, 1986b.

Atkinson, R.: A structure-activity relationship for the estimation of rate constants for the gas-phase reactions of OH radicals with organic compounds, Int. J. Chem. Kinet., 19, 799–828, https://doi.org/10.1002/kin.550190903, 1987.

Belsito, D., Bickers, D., Bruze, M., Calow, P., Greim, H., Hanifin, J. M., Rogers, A. E., Saurat, J. H., Sipes, I. G., and Tagami, H.: A toxicologic and dermatologic assessment of cyclic and non-cyclic terpene alcohols when used as fragrance ingredients, Food Chem. Toxicol., 46, S1–S71, https://doi.org/10.1016/j.fct.2008.06.085, 2008.

Bennett, J. E. and Summers, R.: Product Studies of the Mutual Termination Reactions of sec-Alkylperoxy Radicals: Evidence for Non-Cyclic Termination, Can. J. Chem., 52, 1377–1379, https://doi.org/10.1139/v74-209, 1974.

Bräuer, P., Mouchel-Vallon, C., Tilgner, A., Mutzel, A., Böge, O., Rodigast, M., Poulain, L., van Pinxteren, D., Wolke, R., Aumont, B., and Herrmann, H.: Development of a protocol for the auto-generation of explicit aqueous-phase oxidation schemes of organic compounds, Atmos. Chem. Phys., 19, 9209–9239, https://doi.org/10.5194/acp-19-9209-2019, 2019.

Buxton, G. V., Greenstock, C. L., Helman, W. P., and Ross, A. B.: Critical Review of rate constants for reactions of hydrated electrons, hydrogen atoms and hydroxyl radicals (OH/O− in Aqueous Solution, J. Phys. Chem. Ref. Data, 17, 513–886, https://doi.org/10.1063/1.555805, 1988.

Carlton, A. G., Christiansen, A. E., Flesch, M. M., Hennigan, C. J., and Sareen, N.: Multiphase Atmospheric Chemistry in Liquid Water: Impacts and Controllability of Organic Aerosol, Acc. Chem. Res., 53, 1715–1723, https://doi.org/10.1021/acs.accounts.0c00301, 2020.

Ceacero-Vega, A. A., Ballesteros, B., Bejan, I., Barnes, I., Jiménez, E., and Albaladejo, J.: Kinetics and Mechanisms

of the Tropospheric Reactions of Menthol, Borneol, Fenchol, Camphor, and Fenchone with Hydroxyl Radicals (OH) and Chlorine Atoms (Cl), J. Phys. Chem. A, 116, 4097–4107, https://doi.org/10.1021/jp212076g, 2012.

Chandler, D.: Interfaces and the driving force of hydrophobic assembly, Nature, 437, 640–647, https://doi.org/10.1038/nature04162, 2005.

Chen, H., Su, X., He, J., Zhang, P., Xu, H., and Zhou, C.: Investigation on combustion characteristics of cyclopentanol/diesel fuel blends in an optical engine, Renew. Energ., 167, 811–829, https://doi.org/10.1016/j.renene.2020.11.155, 2021.

Cheng, Y., Zheng, G., Wei, C., Mu, Q., Zheng, B., Wang, Z., Gao, M., Zhang, Q., He, K., Carmichael, G., Pöschl, U., and Su, H.: Reactive nitrogen chemistry in aerosol water as a source of sulfate during haze events in China, Sci. Adv., 2, 1–11, https://doi.org/10.1126/sciadv.1601530, 2016.

Chin, M. and Wine, P. H.: A Temperature-Dependent Competitive Kinetics Study of the Aqueous-Phase Reactions of OH Radicals with Formate, Formic Acid, Acetate, Acetic Acid, and Hydrated Formaldehyde, Symposium on Aquatic and Surface Photochemistry, at the 203rd National Meeting of the American-Chemical-Society, San Francisco, Ca, April 5–10, WOS:A1994, 85–96, eBook ISBN 9781351069847, https://doi.org/10.1201/9781351069847, 1994.

Claeys, M., Iinuma, Y., Szmigielski, R., Surratt, J. D., Blockhuys, F., Van Alsenoy, C., Bołge, O., Sierau, B., Goìmez-Gonzaìlez, Y., Vermeylen, R., Van der Veken, P., Shahgholi, M., Chan, A. W. H., Herrmann, H., Seinfeld, J. H., and Maenhaut, W.: Terpenylic Acid and Related Compounds from the Oxidation of α-Pinene: Implications for New Particle Formation and Growth above Forests, Environ. Sci. Technol., 43, 6976–6982, https://doi.org/10.1021/es9007596, 2009.

Das, P., Das, P. K., and Arunan, E.: Conformational Stability and Intramolecular Hydrogen Bonding in 1,2-Ethanediol and 1,4-Butanediol, J. Phys. Chem. A, 119, 3710–3720, https://doi.org/10.1021/jp512686s, 2015.

Doussin, J. F. and Monod, A.: Structure–activity relationship for the estimation of OH-oxidation rate constants of carbonyl compounds in the aqueous phase, Atmos. Chem. Phys., 13, 11625–11641, https://doi.org/10.5194/acp-13-11625-2013, 2013.

Enami, S. and Sakamoto, Y.: OH-Radical Oxidation of Surface-Active cis-Pinonic Acid at the Air–Water Interface, J. Phys. Chem. A, 120, 3578–3587, https://doi.org/10.1021/acs.jpca.6b01261, 2016.

Ervens, B.: Modeling the Processing of Aerosol and Trace Gases in Clouds and Fogs, Chem. Rev., 115, 4157–4198, https://doi.org/10.1021/cr5005887, 2015.

Ervens, B., Gligorovski, S., and Herrmann, H.: Temperature-dependent rate constants for hydroxyl radical reactions with organic compounds in aqueous solutions, Phys. Chem. Chem. Phys., 5, 1811–1824, https://doi.org/10.1039/B300072A, 2003.

Ervens, B., Sorooshian, A., Aldhaif, A. M., Shingler, T., Crosbie, E., Ziemba, L., Campuzano-Jost, P., Jimenez, J. L., and Wisthaler, A.: Is there an aerosol signature of chemical cloud processing?, Atmos. Chem. Phys., 18, 16099–16119, https://doi.org/10.5194/acp-18-16099-2018, 2018.

Fichan, I., Larroche, C., and Gros, J. B.: Water Solubility, Vapor Pressure, and Activity Coefficients of Ter-

penes and Terpenoids, J. Chem. Eng. Data., 44, 56–62, https://doi.org/10.1021/je980070+, 1999.

Fu, P. Q., Kawamura, K., Chen, J., Charrière, B., and Sempéré, R.: Organic molecular composition of marine aerosols over the Arctic Ocean in summer: contributions of primary emission and secondary aerosol formation, Biogeosciences, 10, 653–667, https://doi.org/10.5194/bg-10-653-2013, 2013.

Fuzzi, S., Baltensperger, U., Carslaw, K., Decesari, S., Denier van der Gon, H., Facchini, M. C., Fowler, D., Koren, I., Langford, B., Lohmann, U., Nemitz, E., Pandis, S., Riipinen, I., Rudich, Y., Schaap, M., Slowik, J. G., Spracklen, D. V., Vignati, E., Wild, M., Williams, M., and Gilardoni, S.: Particulate matter, air quality and climate: lessons learned and future needs, Atmos. Chem. Phys., 15, 8217–8299, https://doi.org/10.5194/acp-15-8217-2015, 2015.

Gligorovski, S., Rousse, D., George, C., and Herrmann, H.: Rate constants for the OH reactions with oxygenated organic compounds in aqueous solution, Int. J. Chem. Kinet., 41, 309–326, https://doi.org/10.1002/kin.20405, 2009.

Goldstein, A. H. and Galbally, I. E.: Known and unexplored organic constituents in the earth's atmosphere, Environ. Sci. Technol., 41, 1514–1521, https://doi.org/10.1021/es072476p, 2007.

González-Sánchez, J. M., Brun, N., Wu, J., Morin, J., Temime-Roussel, B., Ravier, S., Mouchel-Vallon, C., Clément, J. L., and Monod, A.: On the importance of atmospheric loss of organic nitrates by aqueous-phase OH oxidation, Atmos. Chem. Phys., 21, 4915–4937, https://doi.org/10.5194/acp-21-4915-2021, 2021.

Guenther, A., Jiang, X., Heald, C. L., Sakulyanontvittaya, T., Duhl, T., Emmons, L., and Wang, X.: The Model of Emissions of Gases and Aerosols from Nature version 2.1 (MEGAN2. 1): an extended and updated framework for modeling biogenic emissions, Geosci. Model. Dev., 5, 1471–1492, https://doi.org/10.5194/gmd-5-1471-2012, 2012.

Hallquist, M., Wenger, J. C., Baltensperger, U., Rudich, Y., Simpson, D., Claeys, M., Dommen, J., Donahue, N. M., George, C., Goldstein, A. H., Hamilton, J. F., Herrmann, H., Hoffmann, T., Iinuma, Y., Jang, M., Jenkin, M. E., Jimenez, J. L., Kiendler-Scharr, A., Maenhaut, W., McFiggans, G., Mentel, T. F., Monod, A., Prévôt, A. S. H., Seinfeld, J. H., Surratt, J. D., Szmigielski, R., and Wildt, J.: The formation, properties and impact of secondary organic aerosol: current and emerging issues, Atmos. Chem. Phys., 9, 5155–5236, https://doi.org/10.5194/acp-9-5155-2009, 2009.

Hart, E. J., Gordon, S., and Thomas, J. K.: A Review of the Radiation Chemistry of Single-Carbon Compounds and Some Reactions of the Hydrated Electron in Aqueous Solution, Radiat. Res., 4, 74–88, 1964.

EPI Suite™: Estimation Program Interface v4.11, https://www.epa.gov/tsca-screening-tools/epi-suitetm-estimation-program-interface, last access: 20 June 2023.

Héral, B., Stierlin, É., Fernandez, X., and Michel, T.: Phytochemicals from the genus Lavandula: a review, Phytochem Rev., 20, 751–771, https://doi.org/10.1007/s11101-020-09719-z, 2021.

Herrmann, H.: Kinetics of aqueous phase reactions relevant for atmospheric chemistry, Chem. Rev., 103, 4691–4716, https://doi.org/10.1021/cr020658q, 2003.

Herrmann, H., Tilgner, A., Barzaghi, P., Majdik, Z., Gligorovski, S., Poulain, L., and Monod, A.: Towards a more detailed description of tropospheric aqueous phase organic chemistry: CAPRAM 3.0, Atmos. Environ., 39, 4351–4363, https://doi.org/10.1016/j.atmosenv.2005.02.016, 2005.

Herrmann, H., Hoffmann, D., Schaefer, T., Bräuer, P., and Tilgner, A.: Tropospheric Aqueous-Phase Free-Radical Chemistry: Radical Sources, Spectra, Reaction Kinetics and Prediction Tools, ChemPhysChem, 11, 3796–3822, https://doi.org/10.1002/cphc.201000533, 2010.

Herrmann, H., Schaefer, T., Tilgner, A., Styler, S. A., Weller, C., Teich, M., and Otto, T.: Tropospheric Aqueous-Phase Chemistry: Kinetics, Mechanisms, and Its Coupling to a Changing Gas Phase, Chem. Rev., 115, 4259–4334, https://doi.org/10.1021/cr500447k, 2015.

Hiura, T., Yoshioka, H., Matsunaga, S. N., Saito, T., Kohyama, T. I., Kusumoto, N., Uchiyama, K., Suyama, Y., and Tsumura, Y.: Diversification of terpenoid emissions proposes a geographic structure based on climate and pathogen composition in Japanese cedar, Sci. Rep., 11, 8307, https://doi.org/10.1038/s41598-021-87810-x, 2021.

Hoffmann, D., Weigert, B., Barzaghi, P., and Herrmann, H.: Reactivity of poly-alcohols towards OH, NO_3 and SO_4^- in aqueous solution, Phys. Chem. Chem. Phys., 11, 9351–9363, https://doi.org/10.1039/B908459B, 2009.

Hunter, J. F., Carrasquillo, A. J., Daumit, K. E., and Kroll, J. H.: Secondary Organic Aerosol Formation from Acyclic, Monocyclic, and Polycyclic Alkanes, Environ. Sci. Technol., 48, 10227–10234, https://doi.org/10.1021/es502674s, 2014.

IUPAC Task Group on Atmospheric Chemical Kinetic Data Evaluation: https://iupac-aeris.ipsl.fr/show_datasheets.php?category=Systematic+OH, last access: 26 September 2023.

Jimenez, J. L., Canagaratna, M. R., Donahue, N. M., Prevot, A. S. H., Zhang, Q., Kroll, J. H., DeCarlo, P. F., Allan, J. D., Coe, H., Ng, N. L., Aiken, A. C., Docherty, K. S., Ulbrich, I. M., Grieshop, A. P., Robinson, A. L., Duplissy, J., Smith, J. D., Wilson, K. R., Lanz, V. A., Hueglin, C., Sun, Y. L., Tian, J., Laaksonen, A., Raatikainen, T., Rautiainen, J., Vaattovaara, P., Ehn, M., Kulmala, M., Tomlinson, J. M., Collins, D. R., Cubison, M. J., Dunlea, J., Huffman, J. A., Onasch, T. B., Alfarra, M. R., Williams, P. I., Bower, K., Kondo, Y., Schneider, J., Drewnick, F., Borrmann, S., Weimer, S., Demerjian, K., Salcedo, D., Cottrell, L., Griffin, R., Takami, A., Miyoshi, T., Hatakeyama, S., Shimono, A., Sun, J. Y., Zhang, Y. M., Dzepina, K., Kimmel, J. R., Sueper, D., Jayne, J. T., Herndon, S. C., Trimborn, A. M., Williams, L. R., Wood, E. C., Middlebrook, A. M., Kolb, C. E., Baltensperger, U., and Worsnop, D. R.: Evolution of Organic Aerosols in the Atmosphere, Science, 326, 1525–1529, https://doi.org/10.1126/science.1180353, 2009.

Klein, R. A.: Hydrogen bonding in diols and binary diol–water systems investigated using DFT methods. II. Calculated infrared OH-stretch frequencies, force constants, and NMR chemical shifts correlate with hydrogen bond geometry and electron density topology. A reevaluation of geometrical criteria for hydrogen bonding, J. Comput. Chem., 24, 1120–1131, https://doi.org/10.1002/jcc.10256, 2003.

Konjeviæ, L., Racar, M., Ilinèiæ, P., and Faraguna, F.: A comprehensive study on application properties of diesel blends with propanol, butanol, isobutanol, pentanol, hexanol, octanol and dodecanol, Energy, 262, 125430, https://doi.org/10.1016/j.energy.2022.125430, 2023.

Kopinke, F.-D. and Georgi, A.: What Controls Selectivity of Hydroxyl Radicals in Aqueous Solution? Indications for a Cage Effect, J. Phys. Chem. A, 121, 7947–7955, https://doi.org/10.1021/acs.jpca.7b05782, 2017.

Kroflič, A., Schaefer, T., Huš, M., Phuoc Le, H., Otto, T., and Herrmann, H.: OH radicals reactivity towards phenol-related pollutants in water: temperature dependence of the rate constants and novel insights into the [OH–phenol]ÿ adduct formation, Phys. Chem. Chem. Phys., 22, 1324–1332, https://doi.org/10.1039/C9CP05533A, 2020.

Kwok, E. S. C. and Atkinson, R.: Estimation of hydroxyl radical reaction rate constants for gas-phase organic compounds using a structure-reactivity relationship: An update, Atmos. Environ., 29, 1685–1695, https://doi.org/10.1016/1352-2310(95)00069-B, 1995.

Leviss, D. H., Van Ry, D. A., and Hinrichs, R. Z.: Multiphase Ozonolysis of Aqueous á-Terpineol, Environ. Sci. Technol., 50, 11698–11705, https://doi.org/10.1021/acs.est.6b03612, 2016.

Lim, Y. B. and Ziemann, P. J.: Effects of Molecular Structure on Aerosol Yields from OH Radical-Initiated Reactions of Linear, Branched, and Cyclic Alkanes in the Presence of NO$_x$, Environ. Sci. Technol., 43, 2328–2334, https://doi.org/10.1021/es803389s, 2009.

Lin, G., Sillman, S., Penner, J. E., and Ito, A.: Global modeling of SOA: the use of different mechanisms for aqueous-phase formation, Atmos. Chem. Phys., 14, 5451–5475, https://doi.org/10.5194/acp-14-5451-2014, 2014.

Mahilang, M., Deb, M. K., and Pervez, S.: Biogenic secondary organic aerosols: A review on formation mechanism, analytical challenges and environmental impacts, Chemosphere, 262, 127771, https://doi.org/10.1016/j.chemosphere.2020.127771, 2021.

Matheson, M. S., Mamou, A., Silverman, J., and Rabani, J.: Reaction of hydroxyl radicals with polyethylene oxide in aqueous solution, J. Phys. Chem. , 77, 2420–2424, https://doi.org/10.1021/j100639a011, 1973.

McGillen, Carter, W. P. L., Mellouki, A., Orlando, J. J., Picquet-Varrault, B., and Wallington, T. J.: Database for the kinetics of the gas-phase atmospheric reactions of organic compounds, Earth Syst. Sci. Data, 12, 1203–1216, https://doi.org/10.5194/essd-12-1203-2020, 2020.

McGillen, M. R., Carter, W. P. L., Mellouki, A., Orlando, J. J., Picquet-Varrault, B., and Wallington, T. J.: Database for the Kinetics of the Gas-Phase Atmospheric Reactions of Organic Compounds, Eurochamp Data Center [data set], https://doi.org/10.25326/mh4q-y215, 2021.

McNeill, V. F.: Aqueous Organic Chemistry in the Atmosphere: Sources and Chemical Processing of Organic Aerosols, Environ. Sci. Technol. , 49, 1237–1244, https://doi.org/10.1021/es5043707, 2015.

McVay, R. and Ervens, B.: A microphysical parameterization of aqSOA and sulfate formation in clouds, Geophys. Res. Lett., 44, 7500–7509, https://doi.org/10.1002/2017gl074233, 2017.

Mekic, M. and Gligorovski, S.: Ionic strength effects on heterogeneous and multiphase chemistry: Clouds versus aerosol particles, Atmos. Environ., 244, 117911, https://doi.org/10.1016/j.atmosenv.2020.117911, 2021.

Mellouki, A., Le Bras, G., and Sidebottom, H.: Kinetics and Mechanisms of the Oxidation of Oxygenated Organic Compounds in the Gas Phase, Chem. Rev., 103, 5077–5096, https://doi.org/10.1021/cr020526x, 2003.

Mellouki, A., Wallington, T. J., and Chen, J.: Atmospheric Chemistry of Oxygenated Volatile Organic Compounds: Impacts on Air Quality and Climate, Chem. Rev., 115, 3984–4014, https://doi.org/10.1021/cr500549n, 2015.

Merz, J. H. and Waters, W. A.: A. – Electron-transfer reactions, The mechanism of oxidation of alcohols with Fenton's reagent, Discuss. Faraday Soc., 2, 179–188, https://doi.org/10.1039/DF9470200179, 1947.

Mitroka, S., Zimmeck, S., Troya, D., and Tanko, J. M.: How Solvent Modulates Hydroxyl Radical Reactivity in Hydrogen Atom Abstractions, J. Am. Chem. Soc., 132, 2907–2913, https://doi.org/10.1021/ja903856t, 2010.

Monod, A. and Doussin, J. F.: Structure-activity relationship for the estimation of OH-oxidation rate constants of aliphatic organic compounds in the aqueous phase: alkanes, alcohols, organic acids and bases, Atmos. Environ., 42, 7611–7622, https://doi.org/10.1016/j.atmosenv.2008.06.005, 2008.

Monod, A., Poulain, L., Grubert, S., Voisin, D., and Wortham, H.: Kinetics of OH-initiated oxidation of oxygenated organic compounds in the aqueous phase: new rate constants, structure–activity relationships and atmospheric implications, Atmos. Environ., 39, 7667–7688, https://doi.org/10.1016/j.atmosenv.2005.03.019, 2005.

Murakami, M. and Ishida, N.: â-Scission of Alkoxy Radicals in Synthetic Transformations, Chem. Lett, 46, 1692–1700, https://doi.org/10.1246/cl.170834, 2017.

Otto, S. and Engberts, J. B. F. N.: Hydrophobic interactions and chemical reactivity, Org. Biomol. Chem., 1, 2809–2820, https://doi.org/10.1039/B305672D, 2003.

Otto, T., Schaefer, T., and Herrmann, H.: Aqueous-Phase Oxidation of Terpene-Derived Acids by Atmospherically Relevant Radicals, J. Phys. Chem. A, 122, 9233–9241, https://doi.org/10.1021/acs.jpca.8b08922, 2018.

Pai, S. J., Heald, C. L., Pierce, J. R., Farina, S. C., Marais, E. A., Jimenez, J. L., Campuzano-Jost, P., Nault, B. A., Middlebrook, A. M., Coe, H., Shilling, J. E., Bahreini, R., Dingle, J. H., and Vu, K.: An evaluation of global organic aerosol schemes using airborne observations, Atmos. Chem. Phys., 20, 2637–2665, https://doi.org/10.5194/acp-20-2637-2020, 2020.

Peduzzi, P., Concato, J., Kemper, E., Holford, T. R., and Feinstein, A. R.: A simulation study of the number of events per variable in logistic regression analysis, J. Clin. Epidemiol., 49, 1373–1379, https://doi.org/10.1016/S0895-4356(96)00236-3, 1996.

Prutz, W. A. and Vogel, S.: Specific rate constants of hydroxyl radical and hydrated electron reaction determined by RCL method, Z. Naturforsch., 31, 1501–1510, https://doi.org/10.1515/znb-1976-1115, 1976.

Pye, H. O. T., Ward-Caviness, C. K., Murphy, B. N., Appel, K. W., and Seltzer, K. M.: Secondary organic aerosol association with cardiorespiratory disease mortality in the United States, Nat. Commun., 12, 7215, https://doi.org/10.1038/s41467-021-27484-1, 2021.

Rauk, A., Boyd, R. J., Boyd, S. L., Henry, D. J., and Radom, L.: Alkoxy radicals in the gaseous phase: â-scission reactions and formation by radical addition to carbonyl compounds, Can. J. Chem., 81, 431–442, https://doi.org/10.1139/v02-206, 2003.

Reuvers, A. P., Greenstock, C. L., Borsa, J., and Chapman, J. D.: Studies on the Mechanism of Chemical Radioprotection by Dimethyl Sulphoxide, Int. J. Radiat. Biol. Relat. Stud. Phys. Chem. Med., 24, 533–536, https://doi.org/10.1080/09553007314551431, 1973.

Richters, S., Herrmann, H., and Berndt, T.: Gas-phase rate coefficients of the reaction of ozone with four sesquiterpenes at 295 ± 2 K, Phys. Chem. Chem. Phys., 17, 11658–11669, https://doi.org/10.1039/C4CP05542J, 2015.

Ross, P. D. and Rekharsky, M. V.: Thermodynamics of hydrogen bond and hydrophobic interactions in cyclodextrin complexes, Biophys. J., 71, 2144–2154, https://doi.org/10.1016/S0006-3495(96)79415-8, 1996.

Russell, G. A.: Deuterium-isotope Effects in the Autoxidation of Aralkyl Hydrocarbons, Mechanism of the Interaction of PEroxy Radicals1, J. Am. Chem. Soc., 79, 3871–3877, https://doi.org/10.1021/ja01571a068, 1957.

Sander, R.: Compilation of Henry's law constants (version 4.0) for water as solvent, Atmos. Chem. Phys., 15, 4399–4981, https://doi.org/10.5194/acp-15-4399-2015, 2015.

Sarang, K., Otto, T., Rudzinski, K., Schaefer, T., Grgiæ, I., Nestorowicz, K., Herrmann, H., and Szmigielski, R.: Reaction Kinetics of Green Leaf Volatiles with Sulfate, Hydroxyl, and Nitrate Radicals in Tropospheric Aqueous Phase, Environ. Sci. Technol., 55, 13666–13676, https://doi.org/10.1021/acs.est.1c03276, 2021.

Sato, K., Jia, T., Tanabe, K., Morino, Y., Kajii, Y., and Imamura, T.: Terpenylic acid and nine-carbon multifunctional compounds formed during the aging of α-pinene ozonolysis secondary organic aerosol, Atmos. Environ., 130, 127–135, https://doi.org/10.1016/j.atmosenv.2015.08.047, 2016.

Schaefer, T., Wen, L., Estelmann, A., Maak, J., and Herrmann, H.: pH- and Temperature-Dependent Kinetics of the Oxidation Reactions of OH with Succinic and Pimelic Acid in Aqueous Solution, Atmosphere, 11, 320–334, https://doi.org/10.3390/atmos11040320, 2020.

Scholes, G. and Willson, R. L.: ã-Radiolysis of aqueous thymine solutions. Determination of relative reaction rates of OH radicals, Trans. Faraday Soc., 63, 2983–2993, https://doi.org/10.1039/TF9676302983, 1967.

Schöne, L., Schindelka, J., Szeremeta, E., Schaefer, T., Hoffmann, D., Rudzinski, K. J., Szmigielski, R., and Herrmann, H.: Atmospheric aqueous phase radical chemistry of the isoprene oxidation products methacrolein, methyl vinyl ketone, methacrylic acid and acrylic acid – kinetics and product studies, Phys. Chem. Chem. Phys., 16, 6257–6272, https://doi.org/10.1039/C3CP54859G, 2014.

Shrivastava, M., Cappa, C. D., Fan, J., Goldstein, A. H., Guenther, A. B., Jimenez, J. L., Kuang, C., Laskin, A., Martin, S. T., Ng, N. L., Petaja, T., Pierce, J. R., Rasch, P. J., Roldin, P., Seinfeld, J. H., Shilling, J., Smith, J. N., Thornton, J. A., Volkamer, R., Wang, J., Worsnop, D. R., Zaveri, R. A., Zelenyuk, A., and Zhang, Q.: Recent advances in understanding secondary organic aerosol: Implications for global climate forcing, Rev. Geophys., 55, 509–559, https://doi.org/10.1002/2016RG000540, 2017.

Sindelarova, K., Granier, C., Bouarar, I., Guenther, A., Tilmes, S., Stavrakou, T., Müller, J. F., Kuhn, U., Stefani, P., and Knorr, W.: Global data set of biogenic VOC emissions calculated by the MEGAN model over the last 30 years, Atmos. Chem. Phys., 14, 9317–9341, https://doi.org/10.5194/acp-14-9317-2014, 2014.

Sindelarova, K., Markova, J., Simpson, D., Huszar, P., Karlicky, J., Darras, S., and Granier, C.: High-resolution biogenic global emission inventory for the time period 2000–2019 for air quality modelling, Earth Syst. Sci. Data, 14, 251–270, https://doi.org/10.5194/essd-14-251-2022, 2022.

Smith, I. W. M. and Ravishankara, A. R.: Role of Hydrogen-Bonded Intermediates in the Bimolecular Reactions of the Hydroxyl Radical, J. Phys. Chem. A, 106, 4798–4807, https://doi.org/10.1021/jp014234w, 2002.

Stemmler, K. and von Gunten, U.: OH radical-initiated oxidation of organic compounds in atmospheric water phases: part 1. Reactions of peroxyl radicals derived from 2-butoxyethanol in water, Atmos. Environ., 34, 4241–4252, https://doi.org/10.1016/S1352-2310(00)00218-1, 2000.

Su, H., Cheng, Y., and Pöschl, U.: New Multiphase Chemical Processes Influencing Atmospheric Aerosols, Air Quality, and Climate in the Anthropocene, Acc. Chem. Res., 53, 2034–2043, https://doi.org/10.1021/acs.accounts.0c00246, 2020.

Swain, C. G. and Lupton, E. C.: Field and resonance components of substituent effects, J. Am. Chem. Soc., 90, 4328–4337, https://doi.org/10.1021/ja01018a024, 1968.

Tsigaridis, K. and Kanakidou, M.: The Present and Future of Secondary Organic Aerosol Direct Forcing on Climate, Curr. Clim. Change Rep., 4, 84–98, https://doi.org/10.1007/s40641-018-0092-3, 2018.

Tsui, W. G., Woo, J. L., and McNeill, V. F.: Impact of Aerosol-Cloud Cycling on Aqueous Secondary Organic Aerosol Formation, Atmosphere, 10, 666–678, https://doi.org/10.3390/atmos10110666, 2019.

von Sonntag, C. and Schuchmann, H.-P.: The Elucidation of Peroxyl Radical Reactions in Aqueous Solution with the Help of Radiation-Chemical Methods, Angew. Chem., Int. Ed. Engl., 30, 1229–1253, https://doi.org/10.1002/anie.199112291, 1991.

Willson, R. L., Greenstock, C. L., Adams, G. E., Wageman, R., and Dorfman, L. M.: The standardization of hydroxyl radical rate data from radiation chemistry, Int. J. Radiat. Phys. Chem., 3, 211–220, https://doi.org/10.1016/0020-7055(71)90023-4, 1971.

Witkowski, B.: Kinetic dataset – aqueous oxidation of aliphatic molecules by hydroxyl radical, RepOD [data set], https://doi.org/10.18150/CPIWK1, 2023.

Witkowski, B. and Gierczak, T.: cis-Pinonic Acid Oxidation by Hydroxyl Radicals in the Aqueous Phase under Acidic and Basic Conditions: Kinetics and Mechanism, Environ. Sci. Technol., 51, 9765–9773, https://doi.org/10.1021/acs.est.7b02427, 2017.

Witkowski, B., Al-sharafi, M., and Gierczak, T.: Kinetics of Limonene Secondary Organic Aerosol Oxidation in the Aqueous Phase, Environ. Sci. Technol., 52, 11583–11590, https://doi.org/10.1021/acs.est.8b02516, 2018a.

Witkowski, B., Jurdana, S., and Gierczak, T.: Limononic Acid Oxidation by Hydroxyl Radicals and Ozone in the Aqueous Phase, Environ. Sci. Technol., 52, 3402–3411, https://doi.org/10.1021/acs.est.7b04867, 2018b.

Witkowski, B., Al-sharafi, M., and Gierczak, T.: Kinetics and products of the aqueous-phase oxidation of â-caryophyllonic acid by hydroxyl radicals, Atmos. Environ., 213, 231–238, https://doi.org/10.1016/j.atmosenv.2019.06.016, 2019.

Witkowski, B., Chi, J., Jain, P., Błaziak, K., and Gierczak, T.: Aqueous OH kinetics of saturated C_6–C_{10} dicarboxylic acids under acidic and basic conditions between 283 and 318 K; new structure-activity relationship parameters, Atmos. Environ., 267, 118761, https://doi.org/10.1016/j.atmosenv.2021.118761, 2021.

Witkowski, B., al-Sharafi, M., Błaziak, K., and Gierczak, T.: Aging of α-Pinene Secondary Organic Aerosol by Hydroxyl Radicals in the Aqueous Phase: Kinetics and Products, Environ. Sci. Technol., 57, 6040–6051, https://doi.org/10.1021/acs.est.2c07630, 2023.

Xu, L., Du, L., Tsona, N. T., and Ge, M.: Anthropogenic Effects on Biogenic Secondary Organic Aerosol Formation, Adv. Atmos. Sci., 38, 1053–1084, https://doi.org/10.1007/s00376-020-0284-3, 2021.

Yamabe, S. and Yamazaki, S.: A DFT study of proton transfers for the reaction of phenol and hydroxyl radical leading to dihydroxybenzene and H_2O in the water cluster, Int. J. Quantum Chem., 118, e25510, https://doi.org/10.1002/qua.25510, 2018.

Yasmeen, F., Szmigielski, R., Vermeylen, R., Gómez-González, Y., Surratt, J. D., Chan, A. W. H., Seinfeld, J. H., Maenhaut, W., and Claeys, M.: Mass spectrometric characterization of isomeric terpenoic acids from the oxidation of α-pinene, α-pinene, d-limonene, and Ä3-carene in fine forest aerosol, J. Mass Spectrom., 46, 425–442, https://doi.org/10.1002/jms.1911, 2011.

Zhao, R., Aljawhary, D., Lee, A. K. Y., and Abbatt, J. P. D.: Rapid Aqueous-Phase Photooxidation of Dimers in the α-Pinene Secondary Organic Aerosol, Environ. Sci. Technol. Lett., 4, 205–210, https://doi.org/10.1021/acs.estlett.7b00148, 2017.

Zhou, W., Mekic, M., Liu, J., Loisel, G., Jin, B., Vione, D., and Gligorovski, S.: Ionic strength effects on the photochemical degradation of acetosyringone in atmospheric deliquescent aerosol particles, Atmos. Environ., 198, 83–88, https://doi.org/10.1016/j.atmosenv.2018.10.047, 2019.

Zhu, Y., Tilgner, A., Hoffmann, E. H., Herrmann, H., Kawamura, K., Yang, L., Xue, L., and Wang, W.: Multiphase MCM–CAPRAM modeling of the formation and processing of secondary aerosol constituents observed during the Mt. Tai summer campaign in 2014, Atmos. Chem. Phys., 20, 6725–6747, https://doi.org/10.5194/acp-20-6725-2020, 2020.